ADVANCED DESIGN AND ANALYSIS OF UWB U-SLOT MICROSTRIP PATCH USING THEORY OF CHARACTERISTIC MODES

A DISSERTATION IN
Electrical and Computer Engineering
and
Physics
Presented to the Faculty of the University
of Missouri–Kansas City in partial fulfillment of
the requirements for the degree

DOCTOR OF PHILOSOPHY

BY

MAHRUKH KHAN

M.Sc, University of Engineering and Technology, 2011

Kansas City, Missouri

2017

ADVANCED DESIGN AND ANALYSIS OF UWB U-SLOT MICROSTRIP PATCH USING THEORY OF CHARACTERISTIC MODES

Mahrukh Khan, Candidate for the Doctor of Philosophy Degree

University of Missouri – Kansas City, 2017

ABSTRACT

Ultra wide band is rapidly advancing as a high data rate wireless communication technology. As is the case in conventional wireless communication systems, an antenna also plays a very crucial role in UWB systems. However, there are more challenges in designing a UWB antenna than a narrow band one. A suitable UWB antenna should be capable of operating over an ultra-wide bandwidth as allocated by the FCC. At the same time, satisfactory radiation properties over the entire frequency range are also necessary.

This thesis focuses on UWB antenna design and analysis. Studies have been undertaken covering the areas of UWB fundamentals and antenna theory. In recent years, the U-slot patch antenna established itself as a versatile, low profile and cost effective antenna that can be fine-tuned for ultra-wideband operations. The main objective of this thesis is to propose an effective practical design procedure to design U-Slot antenna and provide physical insight into the design using full wave analysis methods.

This research work focuses on developing a novel scheme to design wideband U-Slot antenna. To validate the design technique antenna is fabricated and measured results are compared with the simulated to assess the performance. .

In this dissertation, effect of reactive loading on probe fed, single layer, U-Slot loaded microstrip antenna is investigated using Theory of Characteristic Modes (TCM). Detailed analysis of reactive loading due to feed location and arm-angle variation is presented.

Optimized reactive loading has been shown to produce a modified U-Slot structure without increasing any cost and complexity. The optimized loaded antennas are wideband with a relatively stable radiation pattern. Furthermore, we propose an optimization guideline for a wide band design with stable radiation patterns.

APPROVAL PAGE

The faculty listed below, appointed by the Dean of the School of Graduate Studies, have examined a dissertation titled "Advanced Design and Analysis of UWB U-slot Microstrip Patch Using Theory of Characteristic Modes", presented by Mahrukh Khan, candidate for the Doctor of Philosophy degree, and hereby certify that in their opinion it is worthy of acceptance.

Supervisory Committee

Deb Chatterjee, Ph.D., Committee Chair
Department of Computer Science & Electrical Engineering

Ghulam M. Chaudhry, Ph.D.
Department of Computer Science & Electrical Engineering

Masud H Chowdhury, Ph.D.
Department of Computer Science & Electrical Engineering

Anthony Caruso, Ph.D.
Department of Physics and Astronomy

Da Ming Zhu, Ph.D.
Department of Physics and Astronomy

CONTENTS

ILLUSTRATIONS

Figure Page

TABLES

ACKNOWLEDGEMENTS

First, I would like to thank God for blessing me with the completion of this dissertation. I wish to express my sincere gratitude to my supervisor, Dr. Deb Chatterjee, for his guidance, support and encouragement. His knowledge and motivation inspired me in many ways and helped me through the hurdles I encountered during my tenure in the PhD program.

I am also grateful to Dr. Ghulam Chaudhry, Dr. Masud Chowdhury, and Dr. Anthony Caruso and Dr. Da Min Zhu for serving on my supervisory committee and for their valuable inputs on my research.

I want to say thanks to my father for encouraging me to see dreams and follow them. I cannot thank enough to my mother for being there in all my difficult times. Many thanks are due to my husband and daughter who stood by me, understood my situation and never gave up. It is due to the collective support of my family that I may be able to complete my dissertation.

CHAPTER 1

INTRODUCTION

1.1 Motivation

Ultra-wideband (UWB) antennas have a very wide frequency spectrum. In 2002, the FCC allocated the frequency range between 3.1 and 10.6 GHz for commercial use [1]. By FCC definition, systems with relative bandwidth larger than 20% or an absolute bandwidth larger than 500 MHz are considered UWB systems [1]. Some of the motivation points for UWB research are: (1) Higher data rates per Shannon's channel capacity theorem, which states that the capacity of a wireless channel varies linearly with bandwidth [2]. In other words, higher data rates can be achieved as the bandwidth over which the antenna transmits or receives data increases. (2) UWB communication is very secure. Any interference from other wireless systems will have to cover the entire UWB spectrum evenly to jam the UWB pulse [2]. (3) UWB wireless communication uses very low power transmission levels, which are below acceptable noise floor levels [2]. Therefore, UWB technology does not cause much interference to other wireless communications. (4) UWB communication uses low cost transceivers, which do not require any modulation or demodulation circuitry [2]. (5) Low-profile UWB microstrip patch antennas have promising applications in biomedical imaging. This is because lower frequencies provide good skin penetration and higher frequencies provide good image resolution.

In recent years, the microstrip patch antenna has been fine-tuned for UWB operations [3-13]. It is the purpose of this dissertation to characterize the various

microstrip patch antenna's broadbanding techniques with the purpose of developing design guidelines to aid the antenna design engineer in designing first-pass antenna structures with very wide bandwidth.

1.2 Microstrip Patch Antennas and Broadening Techniques

The Microstrip patch antenna (MSA) was first proposed in the 1953 by Des champs [14], then it was researched more intensely in the 1970s by Munson [15] and Howell [16]. The MSA is a low-profile antenna that, in its basic form, consists of a metallic patch, dielectric substrate, and ground plane, as shown in Fig. 1.1. The patch shape can be square, rectangular, triangular, circular, or other irregular shape. The dielectric substrate can be made of materials with dielectric constant, ε_r, that ranges between 2.2 and 12 [17]. Due to its small physical dimension and low cost, the MSA finds uses in a variety of wireless communication applications, such as cellular phones, RFID, Wi-Fi, Bluetooth, GPS, and body area networks. Other uses include defense applications, such as conformal antennas on missiles and planes. Radar and satellite systems make use of MSA arrays. Biomedical imaging applications have made use of MSAs, especially in breast cancer detection and treatment [18-27]. The MSAs have a number of advantages [28], which are:

- Lightweight.
- Low profile and compact.
- Conformal, meaning they can conform to different shapes as in missiles.
- Low fabrication cost since they utilize the existing and widespread printed-circuit technology.

- Capable of linear and circular polarization.
- Support of dual- and triple-band frequency operations.
- Easily integrated with microwave integrated circuits.

Some of the disadvantages that MSAs suffer from are [28]:

- Narrow bandwidth with the higher dielectric constant substrates.
- Low efficiency due to dielectric and conductor losses.
- Surface wave excitations especially in thicker substrates.
- Low power handling ability.
- Additional radiation from feeds.

1.3 Summary of Contributions

This dissertation presents contributions to the antenna design community, which are presented in the following chapters.

In chapter 2, it is necessary to understand the theoretical concepts that describe U-Slot microstrip patch, Characteristic Mode Analysis, and the Method of Moments; all three of which are discussed in Chapter 2. In chapter 2, we consider the various Characteristic modal formulations, their properties and the methods one can use to compute and analyze these modes.

In chapter 3, characteristic mode analysis of three empirical design techniques for the probe-fed, symmetrically located, U-Slot microstrip patch antenna, on a single layer grounded substrate, is presented with supporting experimental data. The first method (ResF) utilizes the

existence of the four distinct resonant frequencies, while the second one (DI) relies on the property of dimensional invariance, for the design of the U-Slot microstrip patch. In both these methods optimization of the probe location is necessary for further enhancement of the 10 dB return loss bandwidth. The third method (DIResF), that optimally combines the features of the previous two, is presented here and shown to yield better bandwidth performance with minimal or no probe location optimization, and hence is superior to the other two for rapid prototyping. Characteristic mode analysis is carried out for critical parameters such as substrate electrical thickness, slot width, probe radius and feed location variations to assess their dominant influence on characteristics of the versatile U-Slot microstrip patch antenna.

In chapter 4, effect of reactive loading on probe fed, single layer, U-Slot loaded microstrip antenna is investigated using Theory of Characteristic Modes (TCM). Detailed analysis of reactive loading due to feed location and arm-angle variation is presented. It is shown that the eigenvalue behavior of the characteristic modes can be modified by varying reactive loading on the U-Slot antenna. Thus, it is possible to control certain modes such that they resonate in the desired frequency band. These modes can then effectively be excited to achieve the desired antenna performance. In addition, reactive loading helps to move the impedance loop of smith chart in the middle. Optimized reactive loading has been shown to produce a modified U-Slot structure without increasing any cost and complexity. The optimized loaded antennas are wideband with a relatively stable radiation pattern. Furthermore, we propose an optimization guideline for a wide band design with stable radiation patterns.

Finally In chapter 5, we conclude with a list of the major contributions made throughout this thesis. We will also comment on the potential of characteristic mode concepts applied to U-Slot antenna design.

This dissertation incorporates material from previously published papers by the author in accordance with the copyright policies of the Institute of Electrical and Electronics Engineers (IEEE) and the Applied Computational Electromagnetics Society (ACES). Some portion of chapter 2 includes the results and discussions found in [54,87] (© 2016 IEEE). Some portion of chapter 3 includes the results and discussions found in [87] (© 2016 IEEE). Some portion of chapter 4 includes the results and discussions found in [95] (© 2017 IEEE) and [44] (© 2015 IEEE). Some portion of chapter 5 includes the results and discussions found in [85, 86, 88] (© 2016 ACES) and [87, 89] (© 2016 IEEE).

CHAPTER 2

THEORY OF CHARACTERISTICS MODES

2.1 Introduction

The theory of characteristic modes is a valuable tool for antenna analysis, from both the scattering and excitation perspective. The theoretical analysis determines an infinite set of modal currents with corresponding modal fields for any antenna structure. These currents are independent of excitation and form a basis of surface currents for the domain represented by the analyzed surface. Any conceivable surface current that can exist on the surface can be expanded using the basis formed by the modal currents. Modal currents or characteristic currents are defined as the eigen functions of a weighted eigenvalue equation that involves the impedance matrix of the body. For conducting bodies, they have the following properties:

- They are real or equiphasal, over the surface on which they exist.
- They form an orthogonal set over this surface.
- They diagonalize the generalized impedance matrix for this surface.

These properties are suitable for many different applications, including antenna design, far field pattern synthesis and feed placement. With such tantalizing properties such as orthogonality, characteristic modes can be applied in likely many more electromagnetics related areas.

Characteristic fields are defined to be the electromagnetic fields produced by the characteristic currents. They present the following important properties:

- The characteristic electric fields have equiphasal tangential components over the surface of the body.
- They form an orthogonal set over the radiation sphere.
- They diagonalize the scattering matrix for the body.

Modal solutions that can be obtained applying this theory have the next properties:

- Matrix inversion is not required for computation of the currents since generalized impedance matrix is diagonalized.
- Pattern synthesis can be accomplished without matrix inversion, since the scattering matrix is diagonalized.
- The current on the body can be controlled using the method of modal resonance.

Garbacz and Turpin [28], [29], first developed the theory of characteristic modes. Their discoveries led to a fundamental, although impractical, theory for generalized scatterers. While critical in understanding the historical development of CM theory, the theory proposed by Garbacz will not be discussed as it detracts from the main topics of this thesis. Harrington and Mautz [30] proposed the current working model for the theory of characteristic modes. What gave Harrington's approach such an edge was a clear and concise derivation from straightforward electromagnetics principles with an accompanying method [31] with which one could use existing electromagnetics simulation tools to compute the characteristic modes. Using a moment method formulation and the discretized impedance matrix, one can determine the characteristic modes of any perfectly conducting structure. The properties of characteristic modes are what make this type of modal analysis so useful. Due to their orthogonality properties, and the fact that they form a basis that spans all possible radiation modes of the analyzed structure, characteristic modes gives fundamental insight into how antennas radiate.

2.1.1 The Impedance Operator

Consider an arbitrary conducting surface S, situated within an impressed field $_{i}E$ as shown in Figure 4.

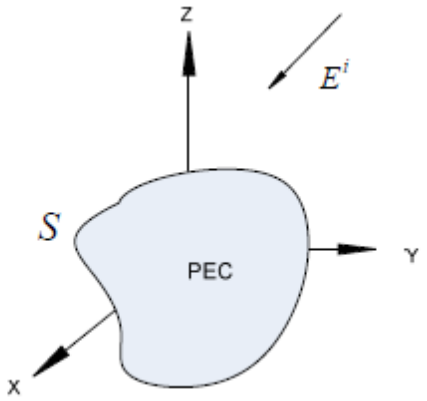

Fig. 2.1– Arbitrary Conducting Surface in an Impressed Field

On the surface of the conductor, the total tangential electric field must be zero. As such, the impressed electric field i E must generate surface currents that force this boundary condition to hold. We define the surface current generated in this way using the operator relationship:

$$[L(\bar{J}) - \overline{E^i}\,]_{tan} = 0 \tag{2.1}$$

The operator L acts on the surface current J and produces a tangential electric field on the surface S that exactly cancels the contribution of the tangential impressed field. The operator L is defined in the following manner:

$$L(\bar{J}) = j\omega\bar{A}(\bar{J}) + \nabla\phi(\bar{J}) \tag{2.2}$$

A(J) is the magnetic vector potential, defined by:

$$A(\bar{J}) = \mu \oiint_S J(r')\psi(r,r')ds' \tag{2.3}$$

$\phi(\bar{J})$ is the electric scalar potential, defined by:

$$\phi(\bar{J}) = \frac{j}{\omega\varepsilon} \oiint_s \nabla' . J(r')\psi(r, r')ds' \tag{2.4}$$

We consider r and r' to be field and source points, with ε, μ, and k as the permittivity, permeability and wave number of free space. Furthermore, we consider ψ (r, r′) being the Green's function of free space, defined as:

$$G(r, r') = \frac{e^{-jk|r-r'|}}{4\pi|r - r'|} \tag{2.5}$$

The operator in Equation 2.3-2 transforms a current density into an electric field quantity, and hence has dimension of impedance. As such, we introduce notation for the tangential operator L:

$$Z(\bar{J}) = [L(\bar{J})]_{tan} \tag{2.6}$$

Where impedance operator in their real and imaginary parts:

$$Z = R + jX \tag{2.7}$$

Both R and X are real operators, and are also symmetric due to the symmetry of Z. Consider the inner product over complex space, defined as the surface integral:

$$\langle \bar{A}.\bar{B} \rangle = \iint_s \bar{A}^* . \bar{B} ds \tag{2.8}$$

Consider the complex power balance of a given impressed surface current J on S.

$$\langle \bar{J}^* . Z\bar{J} \rangle = \langle \bar{J}^*, (R + X)\bar{J} \rangle = \langle \bar{J}^*, R\bar{J} \rangle + j\langle \bar{J}^*, X\bar{J} \rangle$$

(2.9)

The term $\langle \bar{J}^*.Z\bar{J} \rangle$ represents the radiated power associated with the total surface current J on S. This quantity cannot be negative as radiated power must be positive, and is always greater than zero for open structures (since every current radiates some measurable amount of power, however small). These conditions give rise to a positive semi-definite operator R. No further properties than real symmetry exist for the operator X, as reactance can take any value: positive, negative and zero.

2.1.2 Generalized Eigen value Problem

Suppose we now consider our operator Z in the following generalized eigenvalue problem:

$$[\mathrm{Z}][J_n] = v_n[M][J_n] \tag{2.10}$$

where Z is our impedance operator, J_n are the eigenvectors, v_n are the eigenvalues and M is a suitably chosen weighting operator. If M were the identity operator, we would solve the following eigenvalue problem:

$$[\mathrm{Z}][J_n] = v_n[J_n] \tag{2.11}$$

The eigenvalues and eigenvectors would in general be complex, and since [Z] is symmetric, the appropriate orthogonality properties on the surface S defined by [Z] hold. Alternatively, let us consider the operator R as our weighting function. Our eigenvalue problem becomes:

$$[\mathrm{Z}][J_n] = v_n[R][J_n] \tag{2.12}$$

Expanding the operator Z and making the substitution $\nu_n = 1 + j\lambda_n$

$$[R + jX][J_n] = (1 + j\lambda_n)[R][J_n]$$

$$[R] + j[X][J_n] = ([R][J_n] + j\lambda_n)[R][J_n]$$

Canceling like terms, we arrive at the weighted eigenvalue problem:

$$[X][J_n] = \lambda_n[R][J_n] \tag{2.13}$$

Since X and R are real symmetric operators, the resultant eigenvalues and eigenvectors will be purely real. We therefore consider the eigenvectors $[J_n]$ to be the modal currents or eigen currents for the perfectly conducting surface S defined by the operator Z. The significance of the eigenvalues will be discussed shortly.

2.1.3. Characteristic Modal Currents and Normalization:

Since the operators R and X are real symmetric and hence Hermitian, we recognize the following orthogonality properties of the eigen currents with respect to the symmetric and inner products:

$$\begin{aligned} \langle J_m \ . RJ_n \rangle &= \langle J_m{}^* . RJ_n \rangle \\ \langle J_m \ . XJ_n \rangle &= \langle J_m{}^* . XJ_n \rangle \\ \langle J_m \ . ZJ_n \rangle &= \langle J_m{}^* . ZJ_n \rangle \end{aligned} \tag{2.14}$$

where m ≠ n . If the characteristic mode currents are normalized, we can generalize the orthogonality relationships via:

$$\langle J_m \ . RJ_n \rangle = \langle J_m{}^* . RJ_n \rangle = \delta_{mn}$$

$$\langle J_m \ . XJ_n \rangle = \langle J_m{}^* . XJ_n \rangle = \lambda_n \delta_{mn}$$

$$\langle J_m \ . ZJ_n \rangle = \langle J_m{}^* . ZJ_n \rangle = (1 + j\lambda_n)\delta_{mn} \qquad (2.15)$$

where δ_{mn} is the Kronecker delta (0 if m ≠ n , 1 if m = n). All subsequent derivations within this thesis assume normalized current.

2.2 Theory of Charactreistic Mode for Microstrip Patch Antennas

In TCM, Microstrip antenna problem can be formulated as scattering Problem where the surface current distribution on perfectly conducting radiating structure 'S' can be obtained using equivalence principle as shown in Fig. which suggests that in absence of the radiating patch S, the fields due to the impressed current Ji are Ei and Hi [34]. These fields are calculated in presence of the infinite grounded dielectric. Thus, a corresponding EFIE (Electric field integral equation) would read,

$$\overrightarrow{E_i} = \iiint_{V_i} \vec{J}_i . \overline{\overline{G}} \ \mathrm{d}v_i \qquad (2.16)$$

where G is the dyadic Green's function for the current source Ji radiating in presence of the grounded dielectric. Let Es and Hs be the electric and magnetic fields, respectively, due to the equivalent patch surface current Js. The EFIE gives a result similar to (5) that reads,

$$\overrightarrow{E_s} = \iint_S \ \vec{J}_s . \overline{\overline{G}} \ \mathrm{d}s \qquad (2.17)$$

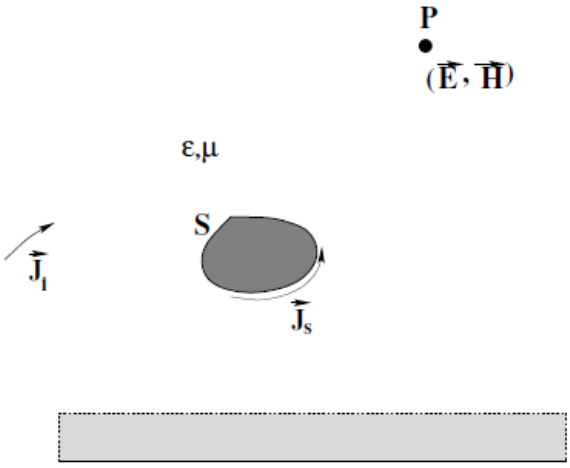

Fig.2.2. Microstrip antenna as a scattering problem.

The unknown current Js=nxHs on the patch surface S, and n is the normal to S. The G in (2.17) is the same as in (2.16), implying that Js radiates in presence of the grounded dielectric.

The enforcement of the boundary conditions on S gives the integral equation:

$$-\vec{E}_s|\tan = -\vec{E}_i|\tan = -\mathcal{L}(\vec{J_s})_i|\tan$$
$$= -Z(\vec{J_s}) \quad = -R(\vec{J_s}) - jX(\vec{J_s}) \tag{2.18}$$

In (2.18) Z is the impedance (continuous) operator. It has been shown in [33, pp. 48–49] from the Poynting power balance equation, minimization of the following functional:

$$\mathcal{F}(\vec{J_s}) = \frac{\langle X(\vec{J_s}), \vec{J_s}* \rangle}{\langle R(\vec{J_s}), \vec{J_s}* \rangle} = \frac{Pstored}{Prad} \tag{2.19}$$

$$P_{stored} = \omega \iiint_V [\mu|H|2 - \mu|E|2] \, d\tau v$$

$$P_{rad} = \iint_s \vec{E} x \vec{H} . \hat{n} ds$$

The minimization of (2.19) can be carried out through the use of Lagrange multipliers and has been worked out in detail in [38, pp. 19–23]. The final result of this procedure is the generalized eigenvalue equation.

$$X(\overrightarrow{J_s}n) = \lambda_n R(\overrightarrow{J_s}\overrightarrow{n}) \tag{2.20}$$

In (2.20), the Jn s are the values of the surface current Js at the extremas associated with the nth Lagrange multiplier _n. The surface current is expanded in the form, [28, Eq. (25)], [29, Eq. (2)]

$$\overrightarrow{J_s} = \sum_n \alpha_n \overrightarrow{J_s}\overrightarrow{n}$$
$$\overrightarrow{J_s}^{n} = \sum_{j=1} I_j \psi_j \tag{2.21}$$

The final result is to calculate the eigenvalues and the eigenvectors in (9) via the resulting discretization of the continuous impedance operator Z in (7). The matrix eigenvalue equation is then given by :

$$[X-\lambda_n R][I]_n = 0 \tag{2.22}$$

The various terms in (11) can be found in [29, Eqs. (5)–(9)] and are omitted here for brevity. where λ_n refers to nth eigen

$$Q_n = 2\omega \frac{\max(W_{e,n}, W_{m,n})}{P_{r,n}} \tag{2.23}$$

Replacing values of $W_{m,n}$ and $W_{e,n}$ from [31] Q_n will become

$$Q_n = \frac{1}{P_{r,n}} [I_n^*] \left[\omega \left(\frac{dX_n}{d\omega}\right) \pm X_n\right] [I_n] \tag{2.24}$$

where X is [30]

$$X = 2\omega(W_m - W_e) \tag{2.25}$$

and from [19] nth eigenvalue has the form

$$\lambda_n = 2\omega\left(W_{m,n} - W_{e,n}\right) \tag{2.26}$$

So,now Qn can be written as

$$Q_n = \frac{1}{P_{r,n}} [I_n^*] \left[\omega \left(\frac{d\lambda_n}{d\omega}\right) \pm \lambda_n\right] [I_n] \tag{2.27}$$

which shows that although current modes are frequency dependent but for very small value of λ_n for n^{th} mode, energy stored and Qn will be small fractional Bandwidth of antenna is defined as [41]

$$BW_n \propto \frac{1}{Q_n} \tag{2.28}$$

which shows that smaller the value of Qn, greater will be the bandwidth contributed by n^{th} mode in total bandwidth of antenna at specific frequency.

2.3 Summary

We have introduced various modal theories, all of which have the critical property of far-field orthogonality. All formulations can be cast into a moment method formulation, which will prove useful when analyzing and designing antennas with the modal theory.

In sections 2.1.1 we discussed the Characteristic Modes (or CM for short). Upon analyzing any arbitrary surface, the computed modes had far-field pattern orthogonality and the ability to expand any surface current on said structure using the modal currents. The modes are computed by solving a generalized eigenvalue problem. The eigenvalues form a useful diagnostic quantity that judges modes suitability for radiation purposes. Moreover, we discussed how one can compute the power radiated and net energy stored associated with each mode in the CM spectrum. This allows us to judge how well we distribute power among the modes given an arbitrary excitation.

CHAPTER 3

DESIGN OF UWB U-SLOT LOADED ANTENNA AND CHARACTREISTIC MODE ANALYSIS

3.1 Introduction

The U-slot microstrip patch antenna [32]–[34] is probably the most useful, practical wideband design ever conceptualized that has witnessed several applications [35]–[39] and spawning of other wideband design topologies starting with the basic U-slot topology. The resources necessary for prototyping a U-slot patch are probably of the same order as required for a traditional probe-fed rectangular patch [40], [41]. While a recent comparison [42] showed that the U-slot patch exhibits superior bandwidth performance, the information gleaned from its circuit analysis [43], or full-wave simulation and experimental results in [44], cannot directly be used for initiating the design of the U-slot microstrip patch from a nominal set of specifications. To that end, information on the design of U-slot patch antennas still remains mostly empirical [34], [46], [47], implying that the limitations of these design methods are not fully understood. Incidentally, the recent studies on the cross-polarization of U-slot patch antennas [45] successfully utilize the empirical design techniques in [46].

The analysis of U-slot in [48] and [49] is more robust than [43], since the input impedance calculation of a probe-fed U-slot is based on segmentation analysis [39],

involving Green's functions for rectangular patch. The major difference between [43] and [49] is that the effects of the substrate permittivity and thickness, in terms of surface wave losses, can be accounted for in [49] through the appropriate expression of the quality (Q) factor. However, even this distinct work does not provide the flexibility for initiating the design of U-slot, as in [46] and [47].

Recent investigations on antenna performance appraisal have focused on characteristic (eigen) mode analysis (CMA) [50]–[56]. CMA is successfully applied for the analysis of planar structures [54] and helps in designing and improving certain characteristics of antennas, e.g., producing circular polarization in U-slot [52], improving the bandwidth of Planar Inverted-F Antenna [55], and so on. Probably one of the earliest applications of CMA was reported in [57]. CMs represent scattering from an object intrinsic to its shape, size, and constitutive electrical parameters when illuminated by an electromagnetic wave [58]–[60]. The CM theory and its various important applications, emphasizing the use of method of moments (MoMs) [61] in the computations, are best summarized in [63]. Recently, the CM theory has been adapted for use in conjunction with combined field integral equation [64] and fast multipole algorithms [65].

The theoretical background of CM is best covered in [69, Ch. 2], following the fundamental theory in [62]. The implementation and the applications of CM have recently been described in [63], [70], and [71]. However, CM has conventionally been used for electrically small or resonant structures; subsequent work in [66] suggests that microstrip patch antennas (that has electrically large grounded substrates) can be analyzed through the use of appropriate layered media Green's function [63, Ch. 3]. The works reported in

[72]–[74] are not directly CM but issues, such as bandwidth, quality factor (Q), and currents, can be analyzed through the CM theory.

This chapter presents a comparative analysis of the existing empirical design techniques for U-slot using the commercially available software FEldberechnung fur Korper mit beliebiger Oberflache (FEKO) [68]. In addition, a new design methodology is proposed and experimentally verified that combines the salient features of the existing design techniques and also provides substantial savings in prototyping of U-slot patch. The CM theory is applied to gain insight into the modal behavior of the two existing empirical design techniques [46], [47] of U-slot and the newly proposed technique.

3.2 Existing Empirical Design Techniques

The geometry of U-slot antenna for both design techniques is shown in Fig. 1, which were simulated using MOM solver option in FEKO [68]. The detailed analysis of both design techniques has been done on four different substrates, which are as follows.

1) $(\varepsilon_r = 2.2;\ h = 3.175)$ mm, $(h\sqrt{\varepsilon_r}/\lambda = 0.1245)$.

2) $(\varepsilon_r = 3.27;\ h = 5.08)$ mm, $(h\sqrt{\varepsilon_r}/\lambda = 0.1536)$.

3) $(\varepsilon_r = 4.4;\ h = 7.62)$ mm, $(h\sqrt{\varepsilon_r}/\lambda = 0.2078)$.

4) $(\varepsilon_r = 9.8;\ h = 12.7)$ mm, $(h\sqrt{\varepsilon_r}/\lambda = 0.3313)$.

The above four designs cover a wide range of thicknesses and dielectric constants. For substrates in 1) and 2), $h/\lambda \approx 0.084$, and for substrates defined in 3) and 4), $h/\lambda \approx 0.1$. The various substrate thickness values were obtained from the manufacturer's (Rogers Corp.) data sheet.

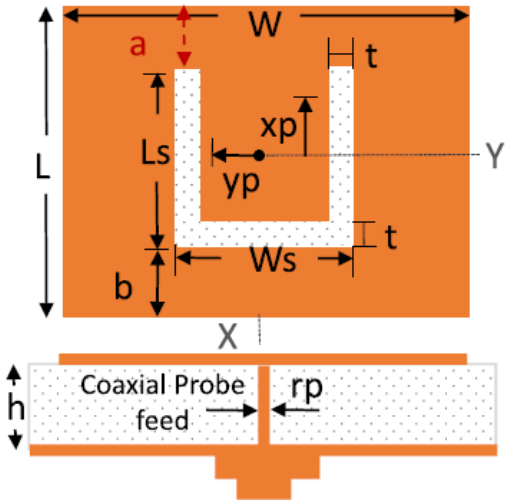

Fig.3.1. U-Slot Loaded Microstrip Patch

3.2.1. Method of Dimensional Invariance [16]

This empirical design technique is based on the observation that for a symmetrically located U-slot, with respect to the rectangular patch, its dimensions remain invariant or bear a constant relationship between them, as shown in Table3.1. The $\varepsilon_r \approx 1$ (air/Rohacell) [1], where *W/L* = 1.385, is an exception, because in this case, no surface waves are excited. Beyond ε_r= 9.8, no data are provided in Table 3.1 increased surface wave losses resulting in reduced radiation efficiency.

To gainfully utilize the information in Table 3.1 for initiating the first-pass design of a U-slot, one notes that all that is needed is the length, *L*, of a rectangular patch of overall dimensions *W*×*L*, as shown in Fig. 3.1, following the procedure in [71, pp. 265–268] and [41, pp. 60–61]. One can then determine the remaining dimensions of the symmetrically located U-slot in Fig. 3.1 using the invariance in the ratios of the dimensions provided in Table 3.1 [77]. An improvement in bandwidth can be achieved choosing a ratio of *W/L* ≈ 1.5 [40, p. 290], and

this is demonstrated from the return loss results shown in Fig. 2. This increase in bandwidth is evident by the following relation [40, p. 283, eq. (4.72a)]:

$$\text{BW} \propto \frac{W}{L} \tag{3.1}$$

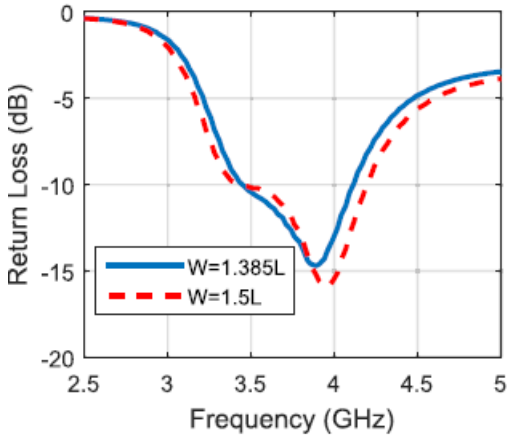

Fig.3.2. Return loss of U-slot antenna using DI on (ε_r= 4.4; h = 7.62 mm) using infinite ground plane.

An important consideration for wideband patch design is the optimization of probe location. The first-pass design, as mentioned earlier, does not contain this information. This optimization process increases the cost of the design cycle and may also markedly affect the cross-polar components in the radiated field, because probe location affects patch surface current distribution, which could radiate undesired cross-polar fields.

Table 3.1: U-slot microstrip patch antenna dimensions [47] (© 2003 ACES)

1.00	1.765	1.515	0.835	4.237	0.13	3.203
2.33	1.383	1.445	0.777	4.5	0.144	2.573
3.27	1.383	1.443	0.772	4.49	0.147	2.568
4.0	1.385	1.443	0.776	4.51	0.144	2.573
4.5	1.382	1.440	0.771	4.53	0.1441	2.566
6.0	1.382	1.440	0.771	4.54	0.144	2.583
9.8	1.384	1.438	0.777	4.48	0.144	2.568

3.2.2 Resonant Frequency Method [15]

This technique is based on the simultaneous excitation of multiple resonant frequencies (ResFs) of U-slot antenna for broadband response [76]. The design method works well for low-permittivity and thin substrates identified in 1) and 2). The ResF method stipulates that the patch design is physically realistic if

$$b > 0 \text{ and } L - Ls > b. \tag{3.2}$$

As ε_r and thickness increase, difference between *L* and *Ls* decreases, which in turn decreases *b*. This feature arises due to the nature of the design relations available in [76]. For high permittivity and thicker substrates, such as in 3) and 4), the condition in (2) is difficult to be satisfied for the adjustable ratios.

$$\frac{L_s}{W} \geq 0.3$$

Or

$$\frac{L_s}{W_s} \geq 0.75$$

These two ratios are a part of the design methodology for U-slot patch antenna, available in [76, Sec. III, step 9)]. As shown in Table 3.2, for higher permittivities (ϵ_r= 9.8), the second condition in (2) is not satisfied, even for permittivity (ϵ_r= 4.4), it is satisfied for very small value of *b*. This suggests that the realization of the broadband characteristics of a U-slot patch antenna is difficult using the ResF method [76] for higher permittivity substrates.

Table. 3.2. ResF method for electrically thicker substrates and high dielectric constants (© 2016 IEEE)

ϵ_r	h	$\frac{L_s - t}{W}$	$\frac{L_s - t}{W_s}$	L-Ls-b	b	fres4-fres2
9.8	12.7	0.47	-	-2.4	0.067	50%
9.8	12.7	-	0.75	-3.6	0.0611	50%
4.4	12.7	0.40	-	1.62	0.154	35%
4.4	12.7	-	1	1.07	0.447	35%

To extend the ResF method [76] to higher permittivity substrates, e.g., 3) and 4), the first condition in (2) is altered by choosing a ≡ b, where *a* shown in Fig. 3.1, and then to recalculate

$$\text{Ls} = \text{L} - 2 \times \text{b} \tag{3.3}$$

Thus, the proposed modification to [46] requires one to determine the parameter *Ls* in Fig. 3.1 directly, and hence, the second criterion in (2) is modified to read

$$L - Ls - b = a \tag{3.4}$$

In Table 3.3, bandwidth comparisons between the original and modified dimensional invariance (DI) and ResF design methods [referred to as DI (mod) and ResF (mod) in all subsequent sections] are shown for low- to high-permittivity substrates. The significant improvement in bandwidth is observed for a U-Slot patch designed on ϵ_r = 9.8 substrate, via the modified ResF method, as shown in Fig. 3.3. The modification to the original DI method was to use *W/L* = 1.5

Table. 3.3. ResF method for electrically thicker substrates and high dielectric constants (© 2016 IEEE)

ϵ_r	h	Dimensional Invariance [47]		Resonant Frequency [46]	
		(Original)	(Modified)	(Original)	(Modified)
2.2	3.175	26.4%	27.52%	26.9%	26.9%
3.27	5.08	18.91%	26%	22.2%	26%
4.4	7.62	17.64%	23%	19%	20.81%
9.8	12.7	25.8%	26.67%	0%	36.9%

For the ResF method, the design modification has been described in the preceding paragraph. By comparison, the corresponding bandwidth results for the DI method are relatively stable, because DI design ratios are independent of the substrate electrical thickness and dielectric constant. However, one common drawback in both the methods is that probe location optimization is necessary to obtain an initial U-slot patch design, which increases optimization cycles and consumes time depending upon machine's specifications.

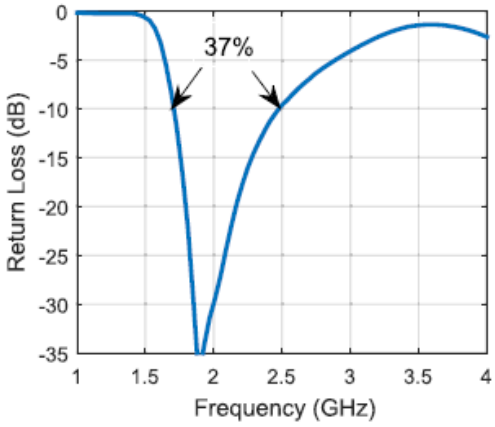

Fig.3.3. Return loss of U-slot antenna using ResF (mod) on (ϵ_r = 9.8; h = 12.7 mm) using an infinite ground plane.

3.2.3. Dimensionally Invariant Resonant Frequency Method

This new design technique is developed here by combining both above-mentioned design techniques, such that minimal optimization of feed location is needed to get optimum bandwidth.

Design Procedure: A flowchart of combined technique, dimensionally invariant ResF (DIResF) method, is shown in Figure 3.4, and the step-by-step design procedure of U-slot antenna is described as follows.

1) Start with the ResF method [46, Sec. III, step 1)], by choosing the substrate ε_r, thickness h, and the desired (resonant) frequency $f\,res3$. Select %BW = $f\,res4 - f\,res2$. Experience suggests that it is safer to choose wider 2:1 VSWR bandwidth than desired.

2) Calculate, following [60, Sec. III], all other patch dimensions.

3) Select *Ls* , such that according to [76, Sec. III, step 9)]

4) The above selection should fulfill the following three conditions.

a) b > 0.

b) We use the information in Table 3.1with the modification

$$3.5 \leq \frac{L_s}{b} \leq 6$$

Note that this criterion provides a range of values for *Ls/b* instead of a fixed number that adds flexibility to the design process.

c) Check if $L - Ls - b > 0$.

If the selection of *Ls* does not satisfy above criteria make b = a.

5) The criterion $1.37 \leq L/Ls \leq 1.49$ is now invoked from the information in Table 3.1. Again, a range of values is obtained here, which like in step 4) adds flexibility to the U-slot patch design.

6) If according to the flowchart in Figure 3.4, the initial design is completed, simulate the design using an appropriate RF software tool, such as FEKO [68] but with the probe location at the center of the patch ($x_p = 0$ and $y_p = 0$).

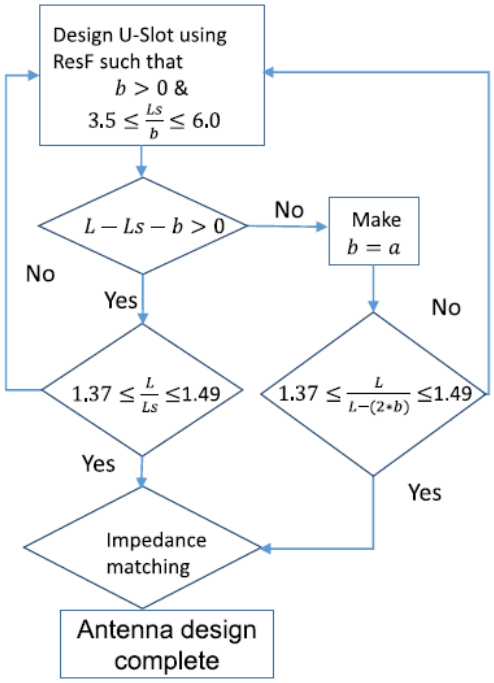

Fig. 3.4. Flowchart of DIResF technique.

Note that information in [46] and [47] has been used in steps 1)–3) and steps 4) and 5), respectively. This approach provides the best values for *Ls* and *b*, and insures realistic design values for all substrates and thicknesses. It is also observed that impedance matching can be controlled by adjusting ratios within those ranges, and hence, feed position is not needed to be optimized for most topologies. Optimum bandwidth and gain pattern at feed position (x_p = 0 and y_p = 0) reduce computational and optimization time. However, it is not a single value ratio, but the small range of ratios that give optimum results. Simulated and measured results to validate this technique are discussed in next section.

3.3 Simulated and Experimental Results

U-slot antenna is designed and simulated for all substrates mentioned in.Tables 3.4–3.6 cover the design values, dimensional ratios, and % bandwidth for DI, ResF, and DIResF. In DI and ResF, feed position needs to be optimized specially for thicker substrates and higher dielectric constants to get broad bandwidth.

Table 3.5 shows the fixed ratio for *Ls/b* and *L/Ls* for all substrates for the DI method. In Table 3.5, for the ResF method, one finds that the variation in the range of ratio *Ls/b* is very large with the increase in substrate thickness and ϵ_r , i.e., 3.1 ≤ *Ls/b* ≤ 15.9; in contrast from Table 3.6, 3.8 ≤ *Ls/b* ≤ 5.13, which is within the specified range shown in Figure 3.4. It can also be observed that % bandwidth for DIResF is more than both existing design methods without optimization of feed location for most cases and slight optimization for 4). Impedance bandwidth behavior for all three methods has been compared in Smith chart plots in Figure 3.5, where the best impedance match is obtained for DIResF among all methods even for thicker substrates and higher dielectric constants.

Table. 3.4. ResF method for electrically thicker substrates and high dielectric constants (© 2016 IEEE)

ϵ_r	h	λ	L	W	Ws	t	b	(xp,yp)	rp	$\frac{L}{Ls}$	$\frac{Ls}{b}$	%BW
2.2	3.175	37.5	10.0793	15.1189	7.5624	0.8461	1.6805	(-0.1,0)	0.3	1.332	4.5	27.52
3.2	5.08	59.8	13.1751	19.7626	9.8979	1.1060	2.1947	(0.2,0)	0.5	1.331	4.5	26
4.4	7.62	76.9	14.6198	21.9296	10.9832	1.2273	2.4353	(0,-2.2)	0.3	1.331	4.5	23
9.8	12.7	120	14.1499	21.2249	10.6125	1.1874	2.3689	(2.3,0)	1	1.333	4.47	26.67

Table. 3.5. ResF method for electrically thicker substrates and high dielectric constants(© 2003 IEEE)

ϵ_r	h	λ	L	W	Ws	t	b	(xp,yp)	rp	$\frac{L}{Ls}$	$\frac{Ls}{b}$	%BW
2.2	3.175	37.5	10.2	19	6.2	0.6	2	(-0.5,0)	0.3	1.4166	3.6	26.9
3.2	5.08	59.8	13.3936	24.7688	9.6644	0.9953	1.3358	(1,0)	0.6	1.385	7.23	26
4.4	7.62	76.9	14.0568	27.4847	10.6764	1.2812	1.6902	(-0.3,0)	0.3	1.3166	6.31	20.8
9.8	12.7	120	13.1345	28.7296	11.6683	1.9986	0.7331	(2.3,0)	1	1.125	15.9	36.9

Table. 3.6. ResF method for electrically thicker substrates and high dielectric constant(© 2003 ACES)

ϵ_r	h	λ	L	W	Ws	t	b	(xp,yp)	rp	$\frac{L}{Ls}$	$\frac{Ls}{b}$	%BW
2.2	3.175	37.5	10.2	19	6	0.6	1.8181	(0,0)	0.3	1.48	3.78	28.5
3.2	5.08	59.8	13.3936	24.7688	9.6365	0.9953	2.0857	(0,0)	0.6	1.452	4.42	29.7
4.4	7.62	76.9	14.0568	27.4847	11.2567	1.2812	1.9975	(0,0)	0.3	1.397	5.03	25.9
9.8	12.7	120	13.1345	28.7296	18.9436	1.9986	1.8418	(0.5,0)	1	1.3897	5.13	37

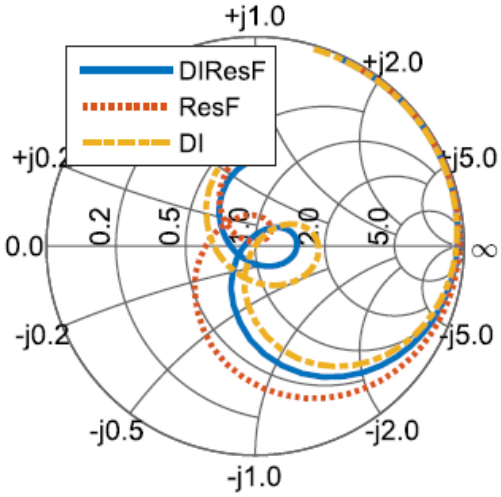

(a)

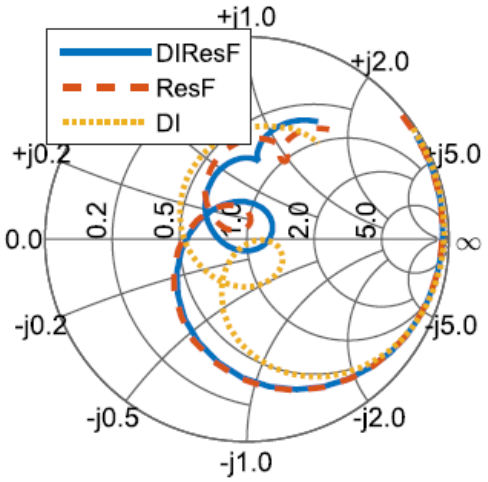

(b)

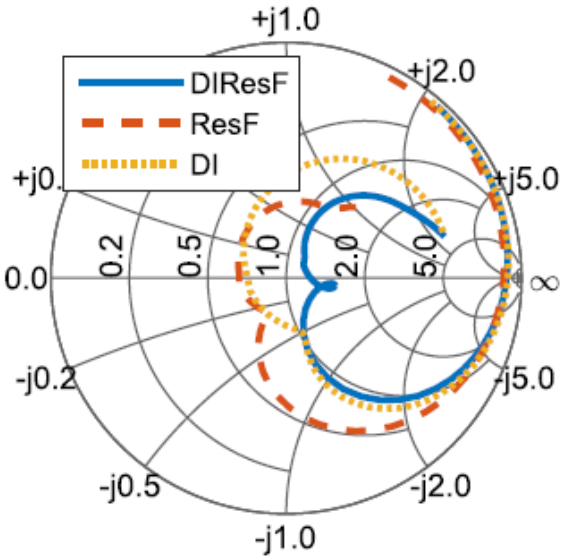

(c)

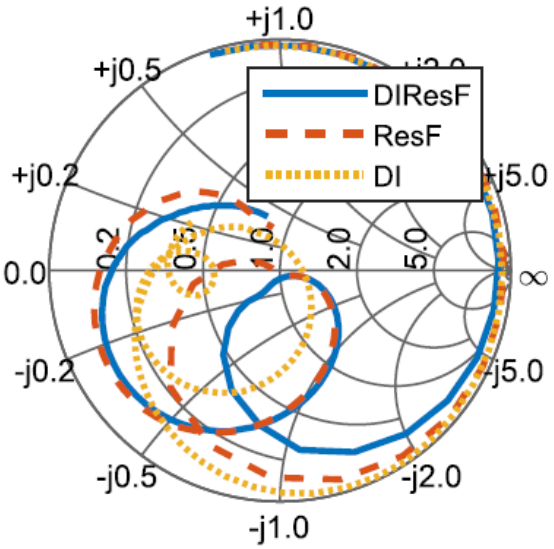

(d)

Fig.3.5. Comparison of simulated results of impedance matching between DI (mod), ResF (mod), and DIResF. (a) ϵ_r = 2.2; h = 3.175 mm. (b) ϵ_r = 3.27; h = 5.08 mm. (c) ϵ_r = 4.4; h = 7.62 mm. (d) ϵ_r = 9.8; h = 12.7 mm.

To experimentally validate the three empirical design approaches, three probe-fed U-slot microstrip patch antennas were fabricated on (ϵ_r = 4.4; h = 11.811 mm, keeping the same $h\sqrt{\epsilon_r}/\lambda$ as in case 3). The thicker substrate was chosen due to maximum frequency limit in available measurement facility. Second, this thickness was readily available and less costly than other customized FR4 substrate panels. The antennas were experimentally characterized for return loss and boresight gain versus frequency. In Fig. 3.6, the designs are shown pictorially. The dimensions of the three U-slot microstrip patch antennas are provided in Table 3.7. The corresponding results for return loss are shown in Fig. 3.7(a)–(c). Fig. 3.8(a)–(c) shows the boresight normalized gain variations with frequency. In all these cases, the simulations were carried out using the FEKO software [68].

One observes excellent agreement for the return loss data in Fig. 3.7 for the three cases obtained for the case of DIResF, which has the widest bandwidth (31%). The simulated [68] peak boresight gain for all three design methods is 5 dBi, which was normalized to 0 dBi in Fig. 3.8(a)–(c), because the EM Scan system used in measurements produced only normalized gain patterns. The boresight gain patterns show diffraction effects due to the edges of the finite size grounded dielectric substrate. The diffraction effects can be accounted for using the formulation in [76], whose implementation is presently beyond the scope of this paper. However, the overall agreement is acceptable.

Table 3.7. U-slot patch designs: ϵ_r = 4.4 and h = 11.811 mm ($h\sqrt{\epsilon_r}/\lambda$ = 0.208). All dimensions in mm(© 2016 IEEE)

Methods	L	W	Ls	Ws	t	b	(xp,yp)	rp	$\frac{L}{Ls}$	$\frac{Ls}{b}$
DI(mod)	22.6	33.9	16.9	13.2	1.89	3.61	(5.1,0)	0.65	1.34	4.6
Resf(mod)	21.7	42.5	17.3	19.8	1.98	1.31	(2,0)	0.65	1.25	13.2
DIResf	21.7	42.5	15.3	19.8	1.98	3.2	(0,0)	0.65	1.41	5.25

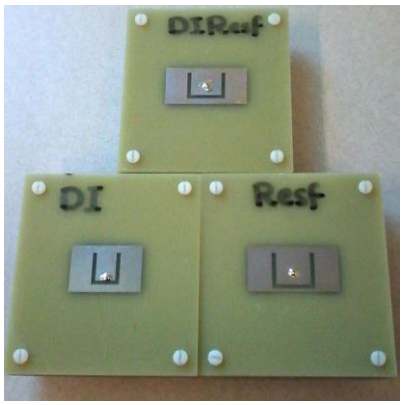

Fig. 3.6. Three prototypes of the probe-fed, U-slot microstrip patch antenna on ϵ_r= 4.4 (FR4) and h = 11.811 mm, finite, grounded dielectric substrate.

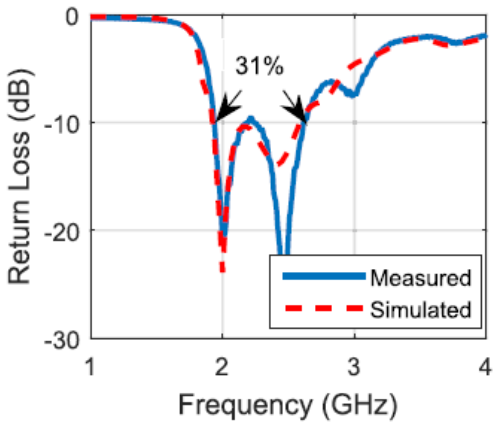

(a)

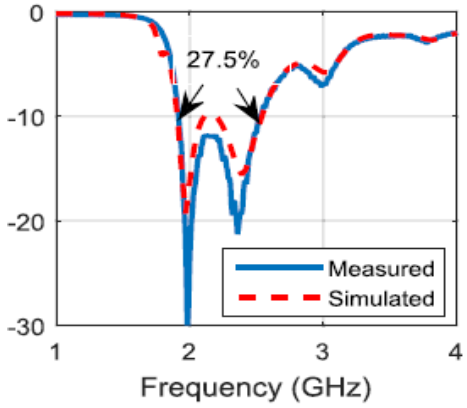

(b)

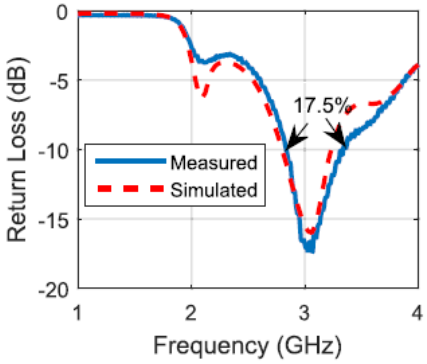

(c)

Fig.3.7. Measured and simulated return loss on (ϵ_r= 4.4; h = 11.811 mm) for (a) DIResF, (b) DI (mod), and (c) ResF (mod).

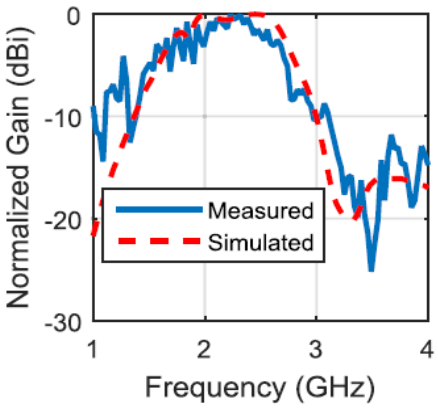

(a)

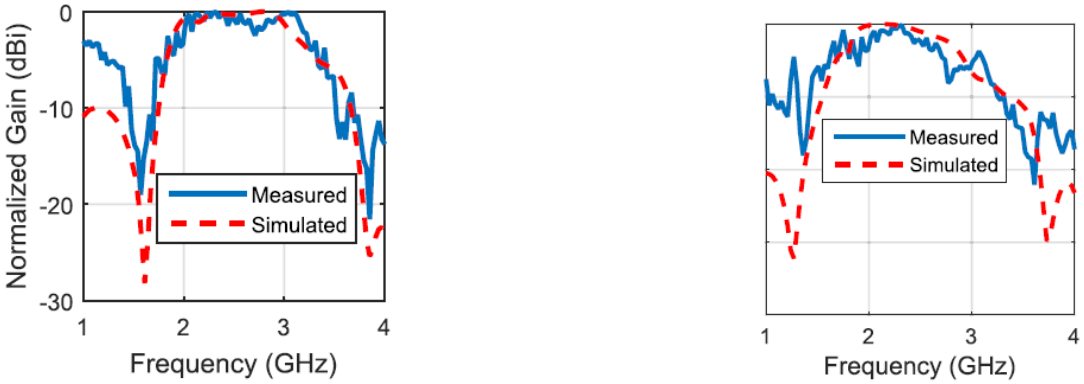

Fig.3.8. Measured and simulated normalized boresight gain (ϵ_r = 4.4; h = 11.811 mm) for (a) DIResF, (b) DI (mod), and (c) ResF (mod)

3.4. Modal Analysis of U-slot Microstrip Patch

CMA for U-slot is carried out for all three-design methods by considering PEC-backed infinite dielectric substrate. Parametric analysis of these design methods helps in understanding their modal contributions for achieving optimum U-slot design. All simulations were done using the commercially available software FEKO [68].

Normalized current distribution of the first six modes of this U-slot antenna on FR-4 substrate with infinite ground is shown in Fig. 3.10. Mode J1 shows the horizontal current distribution which is orthogonal to the direction of main radiating edges (horizontal top

and bottom), and can deteriorate polarization purity if it contributes to the bandwidth [46]. Mode J2 shows the vertical current distribution along the *x*-axis that is intense around the U-slot. Mode J3 shows the intense vertical current confined within the U-slot. Broadband behavior can be observed if modes J2 and J3 contribute to the total impedance bandwidth, but J3 deteriorate polarization purity due to horizontal currents outside the U-slot. Mode J4 does not contribute to the bandwidth because currents tend to cancel each other. Mode J5 is higher order vertical current mode, which is rarely, found to be present in case 3) for DI case and can contribute to the bandwidth. Mode J6 is horizontal currents flowing out in opposite direction from the vertical arms of U-slot. It can be noted that higher order modes contribute in deterioration of gain due to currents in the horizontal direction.

3.4.1. Modal Analysis of Dielectric Thickness ($h\sqrt{\epsilon_r}/\lambda$)

Modal behavior of all design methods on different dielectric thicknesses is shown in Fig.3.11 through modal significance. Modal significance is defined as [57].

$$MS_n = \left|\frac{1}{1 + j\lambda_n}\right| \tag{3.5}$$

Modes with $\lambda_n \rightarrow 0$ give $MS_n \approx 1$, and are good radiators [54]

Table 3.8 shows the modes contributing in total antenna's bandwidth for four cases (mentioned in Section II) in all design methods.

Table 3.8 Modes contributing to the total bandwidth

ϵ_r	h(mm)	DI(mod)	ResF(mod)	DIResF
2.2	3.175	J3,J4	J3,J6	J3,J5
3.27	5.08	J2,J4	J2,J4	J2,J4,J6
4.4	7.62	J1,J2,J3	J2,J3	J2,J3
9.8	12.7	J1,J4	J2,J3	J1,J3

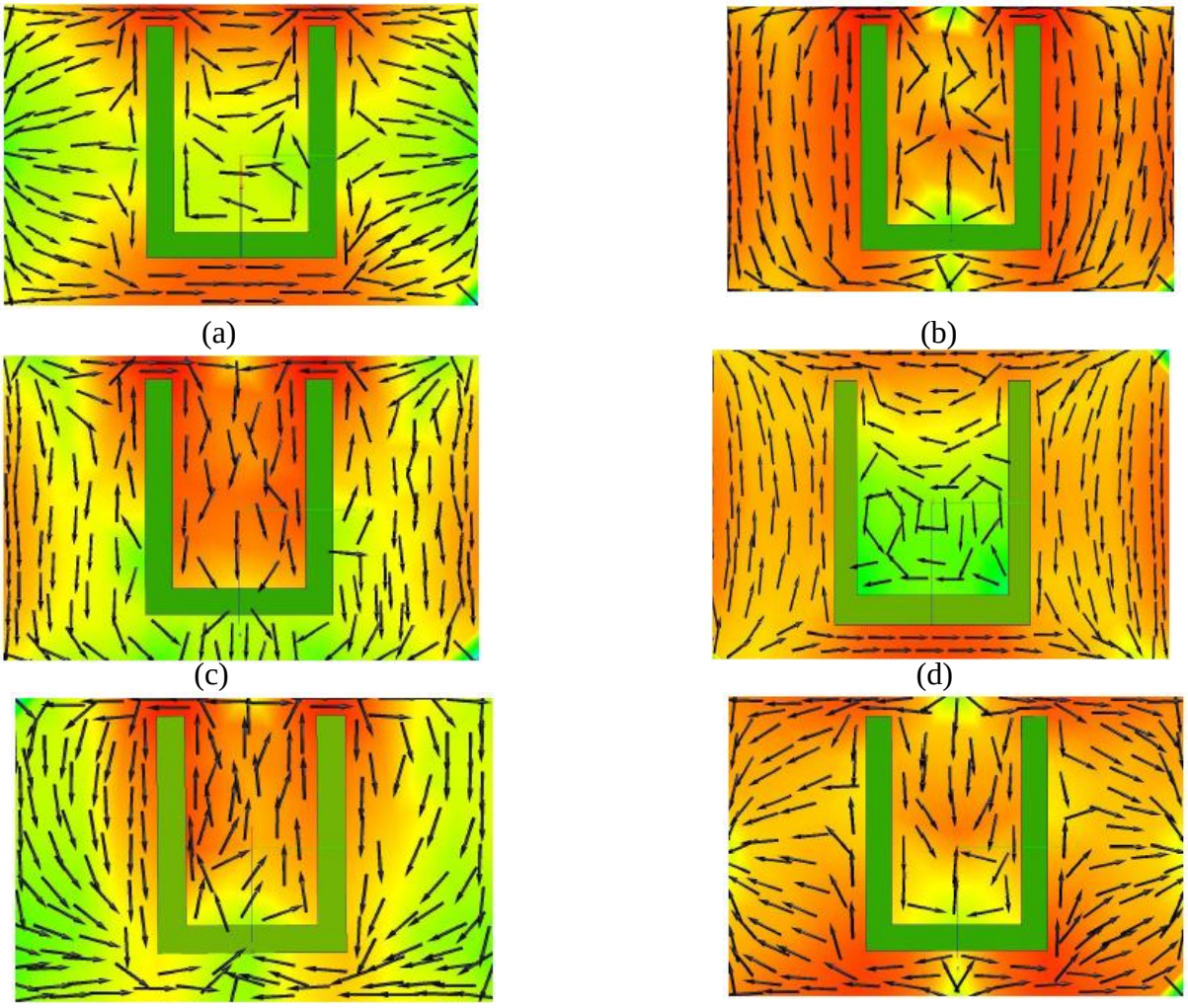

Fig. 3.10 First six CMs of the probe-fed U-slot microstrip patch antenna on (ϵ_r = 4.4; h = 7.62 mm), at a frequency near the resonance of each mode. (a) Mode J1. (b) Mode J2. (c) Mode J3. (d) Mode J4. (e) Mode J5.(f) Mode J6.

These four designs cover the wide range of dielectric thickness, i.e., $0.12 \leq h\sqrt{\epsilon_r}/\lambda \leq 0.33$.In general, ResF modes radiate at lower frequencies than DI for all substrates and DIResF tends to radiate in the middle of the two. In ResF, first mode (J1) is far from the second mode (J2) than in DI, which suggests simultaneous excitation of J1 and J2 is difficult in ResF than in DI.

In first case 1), two modes simultaneously contribute to the bandwidth for all three design methods. Wider bandwidth is observed for a new method DIResF, because J3 and J5 for this method radiate at lower frequencies than other two methods, which increases % bandwidth, as shown in Fig. 3.11(a). For case 2), J2 and J4 are the contributing modes for all methods except for DIResF, in which J6 is also contributing. Current modes in DI radiate at higher frequencies than ResF, as shown in Fig. 3.11(b) that is why ResF for DI is higher than ResF. In DIResF, wider bandwidth is observed than other two methods, because J2 radiated almost at the same frequency as J2 of ResF but J4 radiated near to DI's J4.

Similarly for case 3), J2 and J3 are the contributing modes and J2 of DIResF is excited at lower frequency which is almost the same as ResF, as shown in Fig. 3.11(c), while J3 is excited at the same frequency as J3 of DI, which shows that this method act like ResF at lower ResF, and at higher order mode, it behaves like DI. Hence, the combination of two design methods results in increasing the total impedance bandwidth. Finally, for case 4), J1 and J4 for DI, J2 and J3 for ResF, and J1 and J3 for DIResF, respectively, contribute to the total bandwidth. It has also been observed that for case 4), abrupt anti-resonance is observed (defined according to [41]) for a few current modes in all design methods. This anti-resonant behavior is due to impedance mismatch which is induced due to thick substrate ($d = 0.1\lambda$), high dielectric constant, and probe feed inductance which is apparently not countered with the U-slot's capacitive reactance [32].

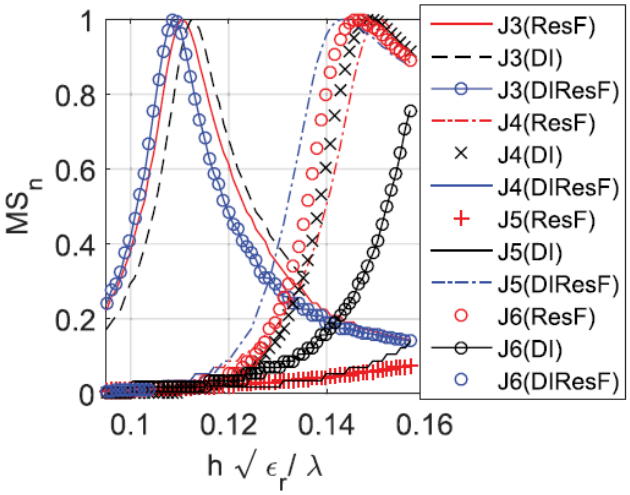

(a) ϵ_r = 2.2; h = 3.175mm

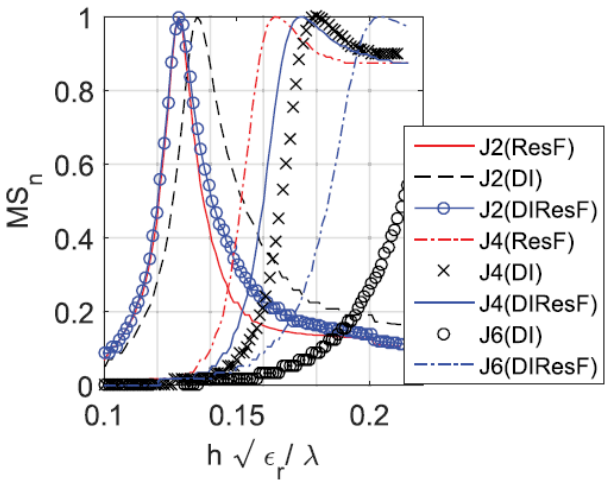

(b) ϵ_r = 3.27; h = 5.08mm

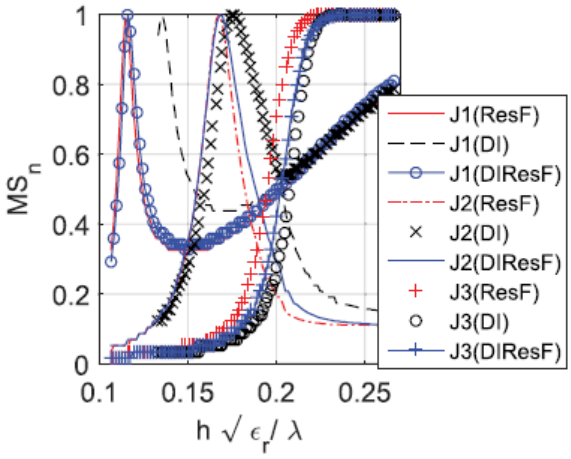

(c) ϵ_r = 4.4; h = 7.62mm

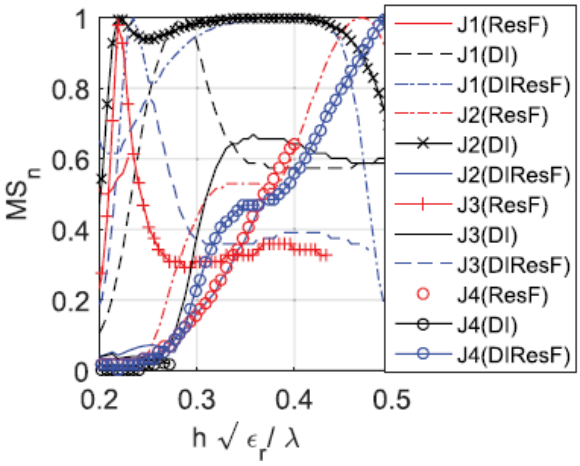

(d) ϵ_r = 9.8; h = 12.7mm

Fig. 3.11. Modal characterization of U-slot for different substrates and dielectric constants: Modal significance vs h$\sqrt{\epsilon_r}$/λ

3.4.2. Modal Analysis of Feed Position Variation

Optimum feed position can excite more than one mode at the same time to give ultrawide bandwidth. The total current distribution on the surface of antenna can be constructed out of set of orthogonal modes [28]

$$J = \sum_n \alpha_n J_n = \sum_n \frac{V_n^i J_n}{1 + j\lambda_n} = \sum_n \frac{\langle J_n, E^i \rangle J_n}{1 + j\lambda_n} \tag{3.6}$$

where a_n is the nth excitation coefficient of the nth mode, which shows that a_n of only a few modes, which have small eigenvalues, can contribute to total radiated field at a specific frequency [44]. V_n is the modal excitation coefficient which account for the way of position, magnitude, and phase of feed effect on each mode contribution to the total current [23].

The effect of antenna feed can be shown through input admittance at feed point (P) [22]

$$Y_{in}[P] = \sum_n \frac{V_n^i J_n(P)}{1+j\lambda_n}(1 - j\lambda_n) \tag{3.7}$$

which is the sum of modal admittances at that point [25]. The effect of feed position is analyzed on (ϵ_r = 4.4; h = 7.62 mm). Optimum feed position for ResF is in the direction of vertical currents, i.e., x-axis, exciting two modes simultaneously to give wide bandwidth. It can also be seen in Fig. 12(a), which shows the real part of total admittance and contribution of modal admittance in the total admittance of U-slot, that J2 and J3 are contributing to the total admittance. Here, J2 and J3 are the vertical current modes, as shown in Fig. 3.11, which is why cross-polar component is less than -40 dB, as shown in Fig. 3.14.

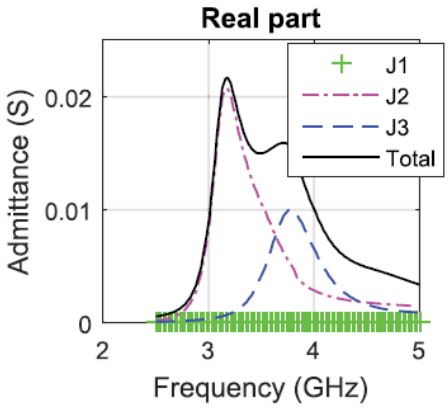

(a)

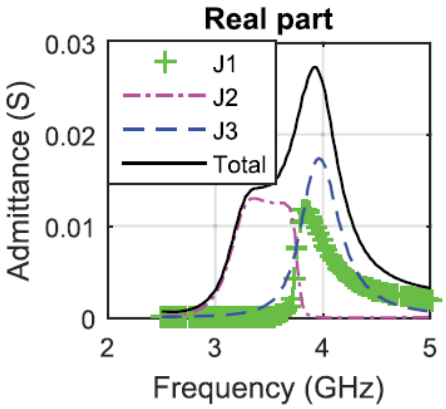

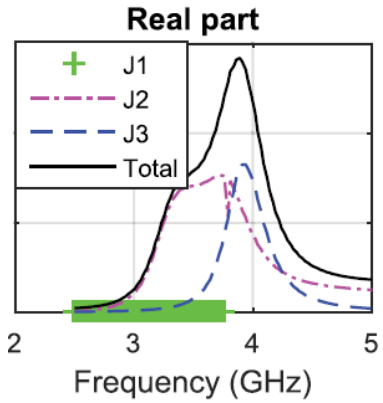

(b) (c)

Fig. 3.12. Contribution of modal admittances (Yn) to the input admittance (Yin) for (a) ResF (mod) at xp=-0.3, yp=0 (b) DI (mod) at xp=0, yp=-2.2 (c) DI at xp=-0.7, yp=0.

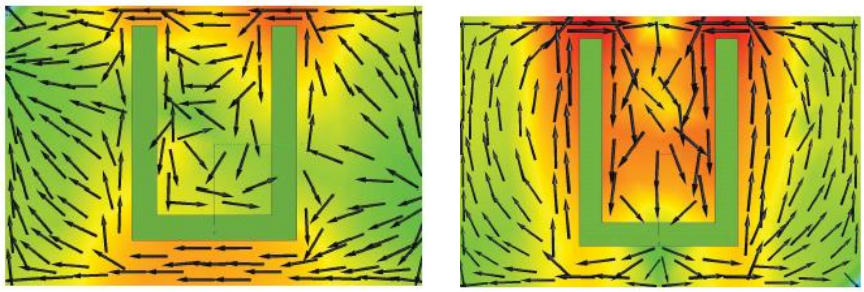

(a) (b)

Fig. 3.13. Mode J2 current distribution on (ϵ_r = 4.4; h = 7.62 mm) at feed position. (a) xp = 0 mm and yp = −2.2 mm. (b) xp = −0.7 mm and yp = 0 mm.

As shown earlier in Fig. 3.11(b) that J1 is near to J2 in DI than other design methods that is why it can contribute in bandwidth along with other modes by optimizing feed location in its current's direction, i.e., *y*-axis. Optimized feed location in the *y*-direction is y*p* = − 2.2 mm that excites three modes J1 (horizontal current mode), J2, and J3 simultaneously, as shown in the admittance graph in Fig.3.12(b). Contribution of three modes increases the bandwidth but this feed position produces diagonal currents for mode J2, as shown in Figure 3.13(a), which deteriorates the polarization purity, as explained in [4].

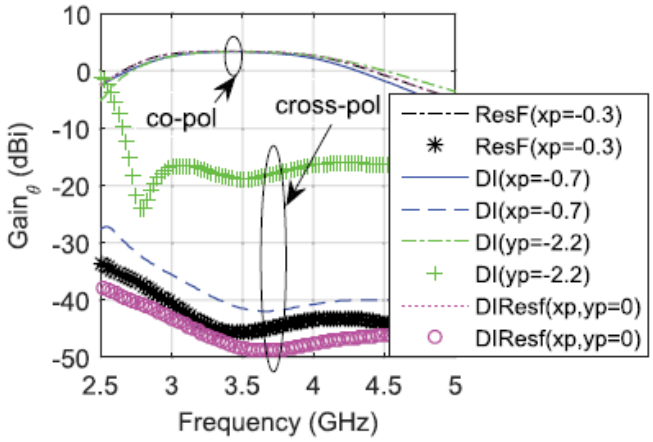

Fig. 3.14. Boresight gain versus frequency for on (ϵ_r = 4.4; *h* = 7.62 mm) for DI (mod), ResF (mod), and DIResF.

3.4.3. Modal Analysis of Probe Radius Variation

Probe radius also affects impedance matching in straight probe-fed microstrip antennas. The selection of probe radius depends on two factors: one is the best impedance matching and the other is the standard available probe radius for measurement. Increase in probe radius decreases probe's inductive reactance [9], which affects the impedance matching of probe-fed antenna especially for thicker substrates.

The effect of probe radius is analyzed using TCMs on (ϵ_r = 4.4; *h* = 7.62 mm) for all design methods. The contribution of current modes in total bandwidth is shown by

VSWR. The effect of change in probe radius on DI is shown in Fig. 3.15. The bandwidth of contributing modes (J1–J3) is increased with the increase in probe radius, but total VSWR deteriorates due to mismatch caused by the reduction in inductive reactance of the probe.

In ResF, J2 and J3 contribute in the total VSWR for the probe radius of 0.3 mm, as shown in Fig. 16. The increase in the probe radius from 0.3 to 0.65 mm increases the bandwidth of modal VSWR's, which causes the increase in total bandwidth, but further increase in probe radius to 1 mm excites higher order modes J4 and J5 instead of J3, which deteriorates impedance matching.

DIResF shows the best behavior for all probe radius among all design methods, as shown in Fig.3.17. It shows good impedance match for thin probes like DI, but with the increase in probe radius, higher order modes J4 and J5 contribute along with J2 to the total bandwidth like ResF but impedance match is better than the ResF case. Hence, the increase in probe radius introduces new higher order modes to contribute in total bandwidth and also affects impedance matching due to the change in probe's inductive reactance.

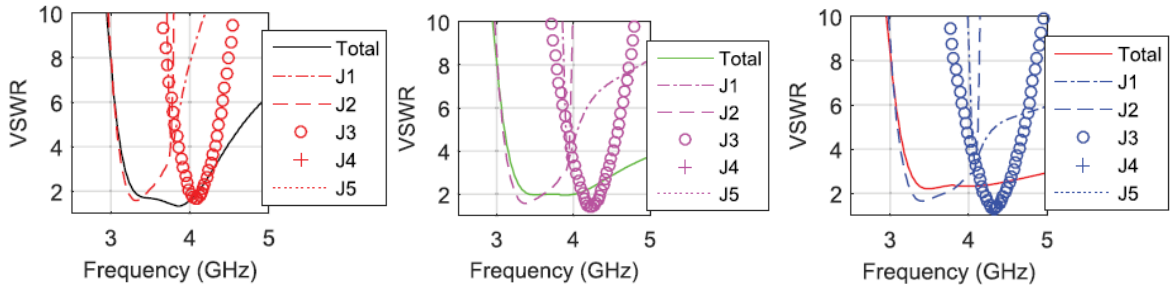

(a) (b) (c)

Fig 3.15 Contribution of modal VSWR to the total VSWR on (ϵ_r = 4.4; h = 7.62 mm) for ResF(mod) at probe radius (a) 0.3 mm, (b) 0.65 mm, and (c) 1 mm.

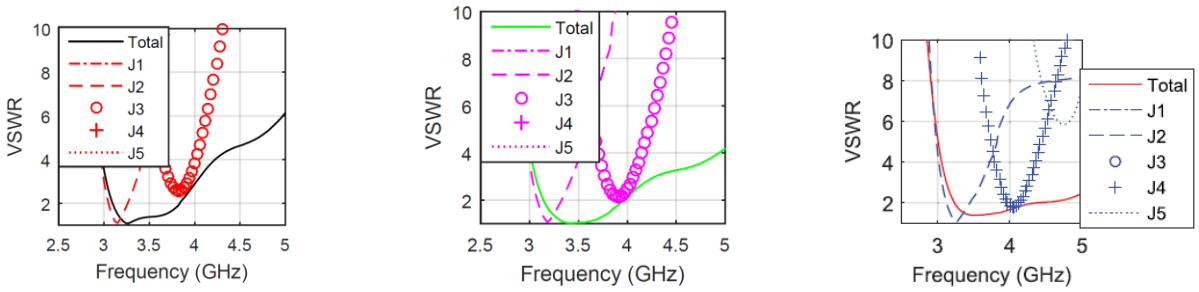

(a) (b) (c)

Fig. 3.16 Contribution of modal VSWR to the total VSWR on (ϵ_r= 4.4; h = 7.62 mm) for ResF(mod) at probe radius (a) 0.3 mm, (b) 0.65 mm, and (c) 1 mm.

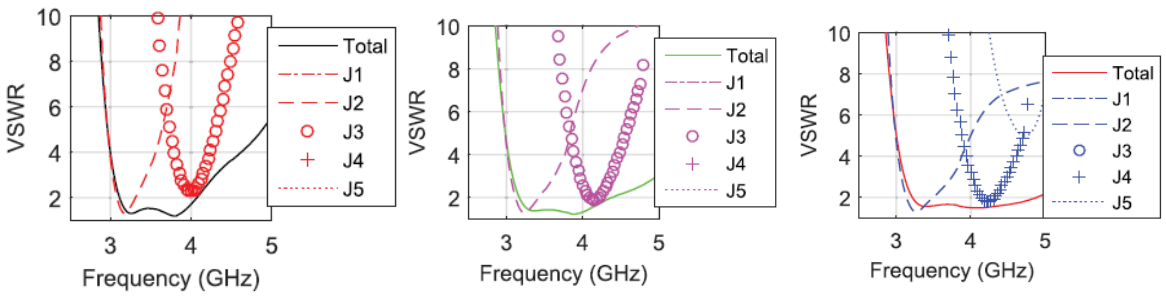

(a) (b) (c)

Fig. 3.17. Contribution of modal VSWR to the total VSWR on (ϵ_r= 4.4; h = 7.62 mm) for DIResF at probe radius (a) 0.3 mm, (b) 0.65 mm, and (c) 1 mm.

3.4.4. Modal Analysis of Slot Thickness/Slot Width Variation

Optimum slot thickness is important for broadband behavior of U-slot, as variation in slot thickness changes impedance matching [12] without introducing new modes. The effect of slot thickness on U-slot is analyzed on (ϵ_r = 4.4,h = 7.62 mm) for all design methods. CMA shows the contribution of modal VSWR of participating current modes (J1–J3) in total VSWR.

Current modes for DI method shows the best behavior at designed value, as shown in Fig. 18, while for thinner slot width, lower order mode J2 contributes more than higher order

mode J3, and as slot width increases, the contribution of J3 increases. Similar trend is observed in ResF, as shown in Fig. 3.19, but for thinner slot width, impedance matching is poorer in ResF than DI, and for thicker slot width, impedance matching is better than DI.

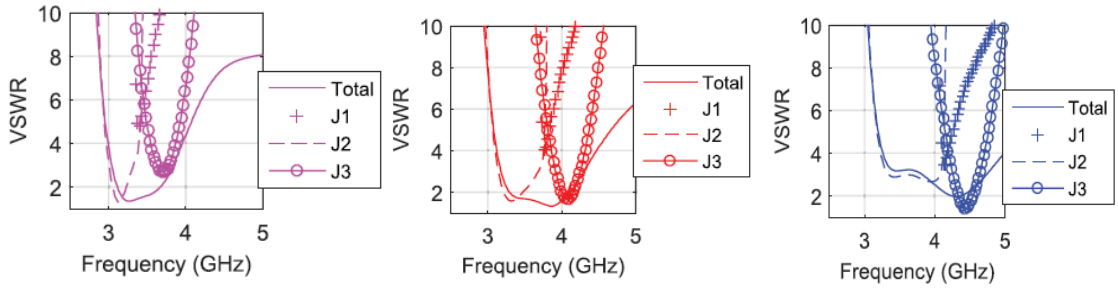

(a) (b) (c)

Fig. 3.18. Contribution of modal VSWR to the total VSWR on (ϵ_r= 4.4; h = 7.62 mm) for DI (mod) at slot width (a) 0.5 mm, (b) 1.28 mm (designed value), and (c) 2 mm.

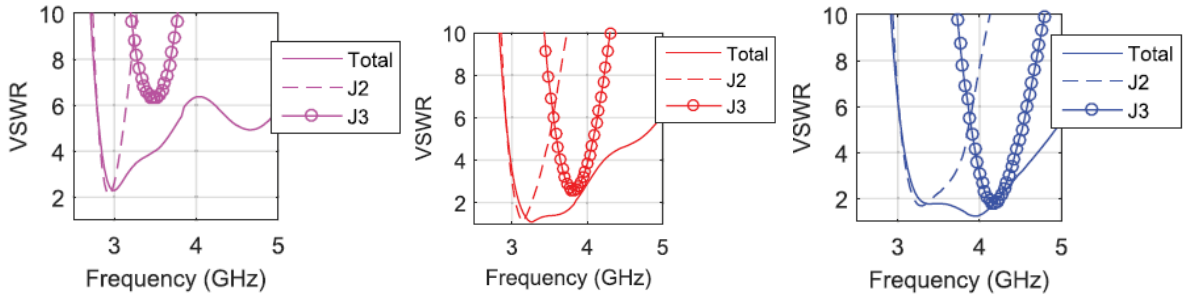

(a) (b) (c)

Fig.3.19. Contribution of modal VSWR to the total VSWR on (ϵ_r = 4.4; h = 7.62 mm) for ResF (mod) at slot width (a) 0.5 mm, (b) 1.28 mm (designed value), and (c) 2 mm.

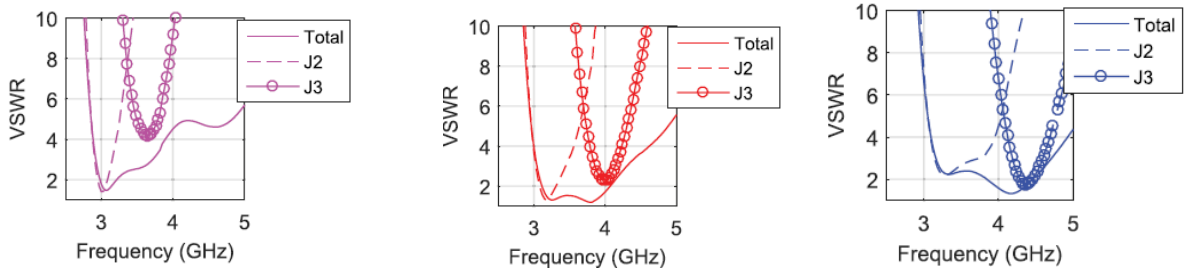

(a) (b) (c)

Fig. 3.20. Contribution of modal VSWR to the total VSWR on (ϵ_r = 4.4; h = 7.62 mm) for DIResF at slot width (a) 0.5 mm, (b) 1.28 mm (designed value), and (c) 2 mm.

3.5. Summary

In this chapter, a new empirical design method DIResF for probe-fed U-slot microstrip patch is developed here, combining the features of the existing design methods, i.e., DI and ResF in such a manner that wideband design can be achieved with minimal or no optimization of probe location. Performance analysis on different substrates reveals that the ResF method works well for low-permittivity and electrically thin substrates, while the DI method works for a much wider range of substrates that are rather arbitrary compared with the ResF. CMA of these methods was carried out with the motivation to understand the modal contributions for achieving wideband designs. CMA for U-slot designs on various dielectric thicknesses indicated that the current modes of DI tend to resonate at higher frequencies than ResF. This difference in modal nature is effectively combined in DIResF technique, because at lower frequency, it resonates near to ResF lower order mode and follows DI pattern at high frequencies to provide the widest 10-dB return loss bandwidth. CMA of feed position for ResF and DI methods shows that bandwidth enhancement due to the excitation of orthogonal current modes can degrade polarization purity, while DIResF gives the best Cross Polar Discrimination without optimizing the feed location. Modal analysis of slot width shows that its variation affects the contribution of participating modes without introducing any new modes for all methods, but DIResF gives optimal design at slot width's design value than other two methods. In all the three cases, an increase in probe radius was seen to introduce higher order modes with an increase in bandwidth. Relevant experimental results for all the three designs have been included which validates the preceding observations. It is thus concluded that DIResF generates the best initial U-slot design that requires minimal optimization for realizing wideband performance.

CHAPTER 4

ANALYSIS OF REACTIVE LOADING IN U-SLOT MICROSTRIP PATCH USING THEORY OF CHARACTERISTIC MODES

Reactive loading of certain parts of an antenna is a powerful technique to control its impedance behavior with respect to the desired frequency bands of operation. Different methods have variously been described in basic microwave literature [1]. The most basic methods simply refer to controlling the entire current distribution on the antenna by reactive elements. More advanced methods such as Theory of Characteristics Modes refers to a modal decomposition of the current distribution of antenna into real wave modes and real value frequencies [2].

TCM has shown promise as a systematic antenna design tool that can not only analyze the antenna designs but can provide a more fundamental understanding of loaded antenna operation [74]-[76]. In [77], a methodology is presented to find a continuous reactive load distribution on the surface of a PEC antenna structure in order to change the resonant frequencies of the characteristic modes. The authors in [78] have presented some techniques to modify the eigenvalues of the characteristic modes and the impedance behavior of the feeding port. TCM analysis of a loaded dipole has been reported to show that higher order modes strongly contribute along with dominant mode as the loading magnitude is increased [79]. In [80], a method to reconstruct the characteristic modes on an antenna from the radiated far field has been presented. In [19], the authors used TCM to provide some design guidelines for the excitation of broadband slotted planar antennas.

In straight probe fed U-Slot microstrip patch, slot loading and feed placement are the most simple and convenient source of reactive loading [82]. A V-Slot is another type of slotted antenna with non-zero arm angle [83]. The arm angle variation enhances its versatility to control the impedance bandwidth. Analysis of inclined slot [82], and V-Slot loaded patch [84] using circuit approach shows change in reactive loading due to slot width variation. Vertical probe feeds are one of the commonly used feeds for planar micro-strip antennas because of their simplicity and ease of fabrication. Optimal feed design and placement can simultaneously excite multiple current modes for broadband behavior [86].

In this chapter, we present a novel optimization procedure for wideband U-Slot antenna after its initial design has been realized in [86]. Optimization procedure use smith chart information to move impedance loop in the middle by controlling reactive loads in U-Slot. With the knowledge of the modal current distribution of the antenna, we have used feed and slot perturbations to control reactive loadings intuitively in order to affect certain modes in the desired way. The slot perturbations are introduced due to unequal variations in inner and outer arm angles of the U-Slot.

This chapter is organized as follows. In Section II, we revisit the TCM and briefly explain the role of reactive loading on the modes. Section III describes the simplistic circuit model of vertical probe fed U-Slot. In Section IV, influence of an arm angle on characteristic modes has been discussed. Section V deals with TCM analysis of vertical probe feed and shows how the feed placements affects the input modal admittance of the U-Slot. Based on TCM analysis of feed and slot, optimization flowchart is proposed to improve impedance matching of the broadband antenna.

4.2. Influence of Reactive Loading on TCM

TCM is conventionally realized through the eigenvalue equation as

$$[X][I_n] = \lambda_n[R][I_n] \tag{4.1}$$

where [X] and [R] are imaginary and real part of MOM impedance matrix Z and _n is the nth eigenvalue of n^{th} eigen vector I_n.

A reactive load distributed on the PEC surface of antenna structure influences the above generalized equation as follows:

$$[X + X_L][I_n] = \lambda_n[R][I_n] \tag{4.2}$$

λ_n is new n^{th} eigen value of loaded system. Comparing above two equation:

$$[\lambda_n]\left[\frac{X_L}{R}\right] = \mu_n \tag{4.3}$$

X_L can be capacitive and inductive as follows:

$$X_L = \begin{cases} 2\pi fL, & X_L > 0 \\ \frac{-1}{2\pi fC}, & X_L < 0 \end{cases} \tag{4.4}$$

This effect of reactive loading on surface current distribution and eigen value behavior of characteristic modes suggests that resonant frequency of characteristic modes can be controlled by reactive loading of antennas. As, mode is resonant at frequency where $\lambda n = 0$, Hence, the increase or decrease in λn directly affects the resonant frequency of current mode.

4.3. U-slot Loaded Microstrip Patch

4.3.1. Equivalent circuit Model of U-slot loaded micro-strip antenna

A simplistic equivalent circuit model of vertical probe fed, U-slot loaded microstrip patch antenna can be modeled as a parallel combination of equivalent circuit of patch and U-Slot as shown in Fig.4.2, where U-Slot loading acts as coupled resonator for

microstrip patch antenna. U-Slot consists of two vertical slots and one horizontal slot. Impedance of horizontal slot 'Z_{HS}' can be read as

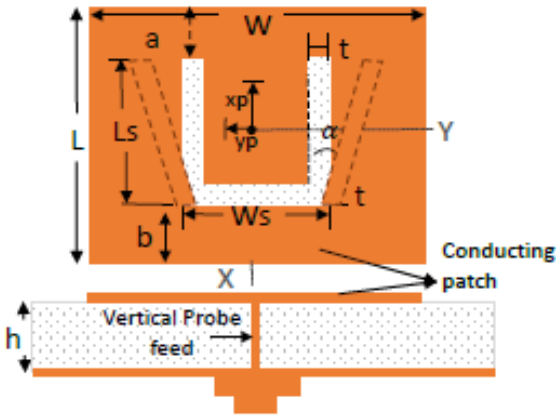

Fig. 4.1. Symmetrically located U-Slot loaded microstrip patch (dashed line shows V-Slot i.e. vertical arm at $\alpha = 0^o$)

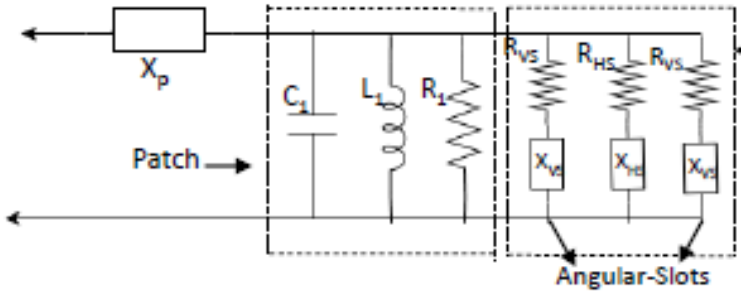

Fig. 4.2. Equivalent circuit model of U-Slot loaded microstrip patch

$$Z_{HS} = R_{HS} + jX_{HS} \tag{4.5}$$

and impedance of vertical slot 'Z_{VS}' is

$$Z_{VS} = R_{VS} + jX_{VS} \tag{4.6}$$

with the total slot impedance 'Z_S' is given by

$$Z_S = 2Z_{VS} + Z_{HS} \tag{4.7}$$

Impedance of unloaded microstrip rectangular patch 'Z_1' is:[12]

$$Z_1 = \frac{1}{\frac{1}{R_1} + j\omega C_1 + \frac{1}{j\omega L_1}} \tag{4.8}$$

The total input impedance 'ZT' of loaded patch can be described as [12]:

$$Z_T = jX_p + \frac{Zs + Z1}{Z_s Z_1} \tag{4.9}$$

where Xp is probe reactance. The total impedance in (9) can be varied by change in Zs and Xp. One of the convenient way of varying Zs i.e slot impedance is to change the arm angle of vertical slots [77]. Non zero and equal arm angles of vertical slot converts U-Slot into V-Slot which is another famous form of Slot loaded antennas. The simplest way to change the feed impedance without affecting the design parameters is to change the feed location. Feed location optimization is an important parameter of optimum U- Slot design.

A U-Slot loaded microstrip antenna is designed on ϵ_r=3.27, h=5.08mm (hp(_r)_ =0.1536) using DIResF method [80] is shown in Fig.4.1. In U-Slot antenna, multiple frequencies resonate simultaneously to give broadband behaviour as shown in Fig.4.3 for _ = 0o. In subsequent sections, we will analyse the influence of reactive loading due to

1) Arm angle

2) Feed location

on the characteristic modes of U-Slot loaded microstrip patch.

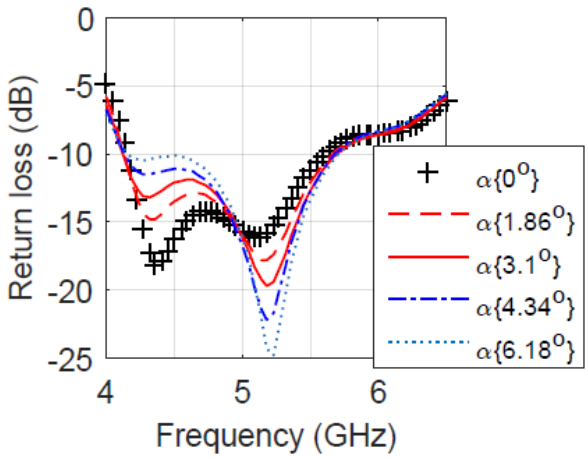

Fig. 4.3. Return loss of U-Slot microstrip patch for different arm angles

(a) (b)

Fig. 4.4. Modified U-Slot patch due to (a) inner arm angle variation (b) outer arm angle variation.

4.4 Influence of Arm-angle on Characteristics Modes

An arm angle α_in U-Slot's vertical arm can be defined as

$$\alpha = tan^{-1}\frac{\Delta t}{L_s} \tag{4.10}$$

where Δt = change in slot width. Effect of an arm angle $'\alpha'$ on U-Slot can be seen in return loss plot in Fig.4.3. It can be noticed that increase in arm angle increases bandwidth at the cost of deterioration in lower resonance frequency matching. To get further insight into the effect of an arm angle, it is divided into two arm angles i.e (i) inner arm angle α_1 and (ii) outer arm angle α_2.

4.4.1 Effect of inner arm-angle variation

To investigate the effect of inner arm angle, outer arm angle is fixed to zero as shown in Fig.4(a). In this case the new slot width ti can be written as

$$t_i = t - \Delta t_i \tag{4.11}$$

where change in slot width is

$$\Delta t_i = L_s tan\alpha_1 \tag{4.12}$$

The variation in 't_i' affects over all impedance because 'X_{VS}' depends on 't' [12]. It can be observed in smith chart in Fig.4.5 that increase in arm angle _1 shifts impedance loop to the capacitive region. There is a limitation in _1 variation i.e ti cannot be negative or $\Delta t_i < t$.

According to (3), capacitive loading (X_L = -1/ (ωC)), (*i.e.*, α_1 variation here) reduces eigenvalue or increases the resonant frequency of the mode. Modal behavior of U-Slot is shown in Fig.4.6. For U-Slot (*i.e.*, $\alpha = 0^0$) J2, J4 are participating current modes . Only few current modes, with low eigen values, participate in impedance bandwidth. Other modes can be neglected as their contribution to the radiated power is rather insignificant. As arm angle increases, resonant frequency of participating current modes tend to increase. It can be noticed that increase in resonant frequency for higher order modes is significant for all arm angles. For $\alpha_1 = 0^0$, J4's λ_n= 0 at 5.6 GHz while for ($\alpha_1 = 5.6^0$), J4's resonant frequency is increased to 5.8 GHz. The significant effect of capacitive loading on higher order mode can be observed in

return loss plot in Fig.4.7 where higher resonant frequency tend to increase significantly with increase in arm angle.

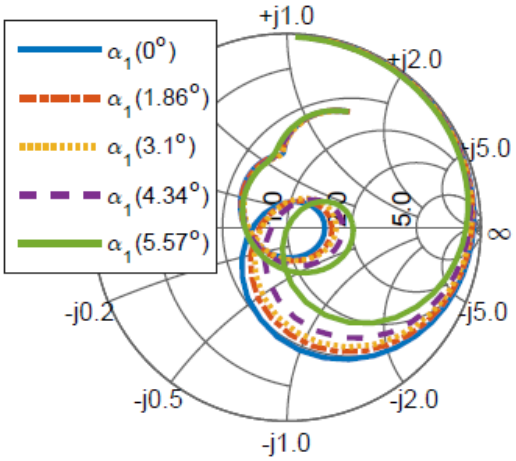

Fig. 4.5. Impedance matching of U-Slot with inner arm-angle variation

It can be noticed that α_1 variation tends to shorten the current path length as shown in Fig.4.8(a) which contributes in increasing the resonant frequency of higher order modes [13]. Return loss in Fig.4.7 shows that for inner arm angle α_1= 4:34° bandwidth is maximum because further increase in angle *i.e.*, α_1 = 5.6° deteriorate impedance matching. Modal behavior in Fig. 6 reveals that for an arm angle α_1= 5.6° higher order and lower order modes are far from each other to contribute simultaneously in bandwidth.

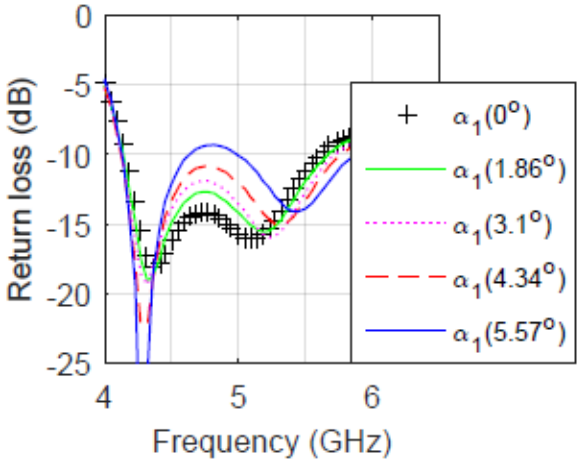

Fig. 4.6. Modal behavior of U-Slot for inner arm angle variation.

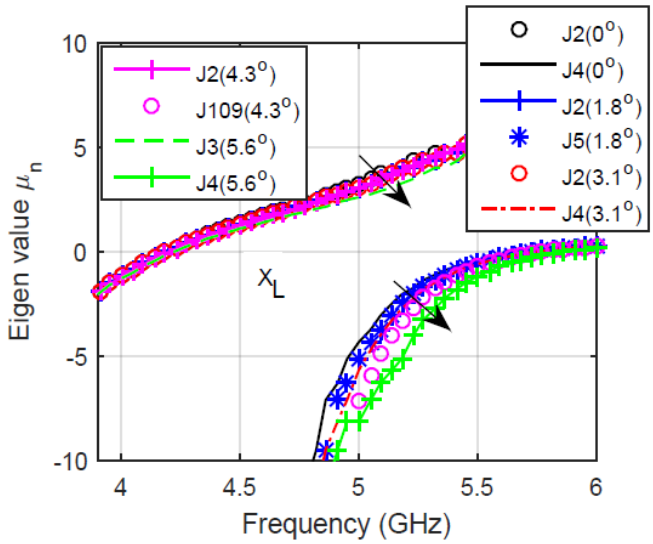

Fig. 4.7. Return loss of U-Slot with inner arm angle variation

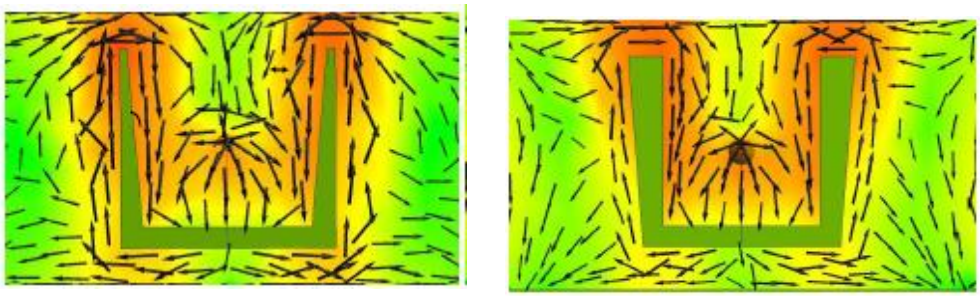

Fig. 4.8. Surface current distribution of U-Slot (modified) patch at resonant mode for (a) _1 variation (b) _2 variation

4.4.2. Effect of outer arm-angle variation

An effect of outer arm angle variation is investigated by keeping inner arm angle fixed as shown in Fig.4.4(b). Outer arm angle variation increases the width of a vertical slot 't' and increase the current path length.

The new width of the slot 't_o' can be recalculated as

$$t_o = t + \Delta t_o \tag{4.13}$$

where Δt_o

$$\Delta t_o = (L_s + t)\tan\alpha_2$$
$$\approx L_s \tan\alpha_2 \quad \text{if } t \ll L_s \tag{4.14}$$

The smith chart in Fig.4.9 shows that increase in arm angle _2 adds inductive behavior in total impedance of V-Slot.

As shown in (3), eigen values increases due to inductive loading (XL = !L),i.e., (increase in _2). Eigen value behaviour of U-Slot in Fig.4.10 shows that eigen value of contributing characteristic modes increases with increase in _2 which in turn causes _n to be zero at lower frequency. This effect is more pronounced for lower order modes than in higher order modes. J2 for _2 = 00 resonates at 4.2 GHz while for _2 = 6:10 it resonates at 4.0 GHz . It is also noticed in return loss plot in Fig. 11 that with increase in _2 impedance matching at lower resonant frequency is reduced which results in narrower impedance bandwidth. For example, for maximum arm angle _2 = 6:18o bandwidth is minimum. The structure of U slot after _2 variation shows that current path is elongated around the vertical slot [78] as shown in Fig.4.8(b) which may also be a reason to increase _ or reduces the resonance frequency of modes.

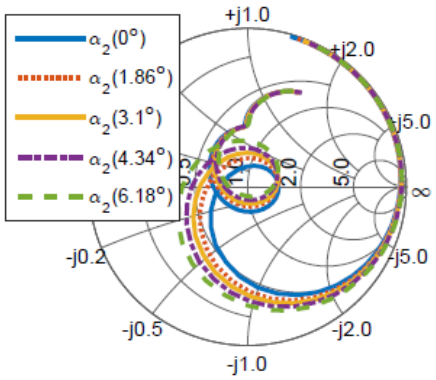

Fig. 4.9. Smith chart of outer-arm variation in U-Slot.

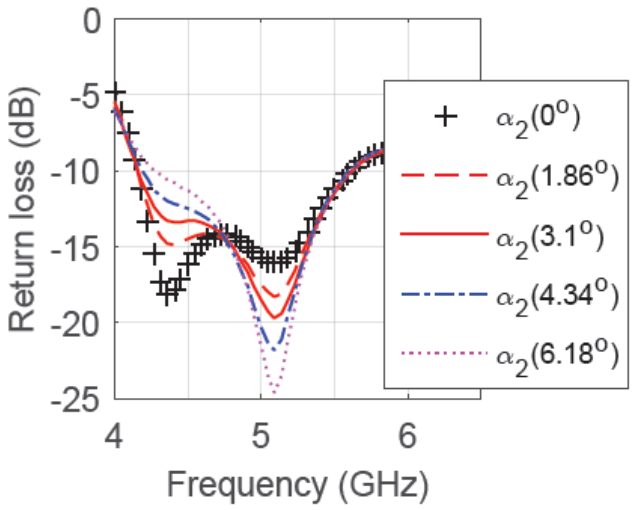

Fig. 4.10. Return loss of U-Slot patch with outer arm-angle variation

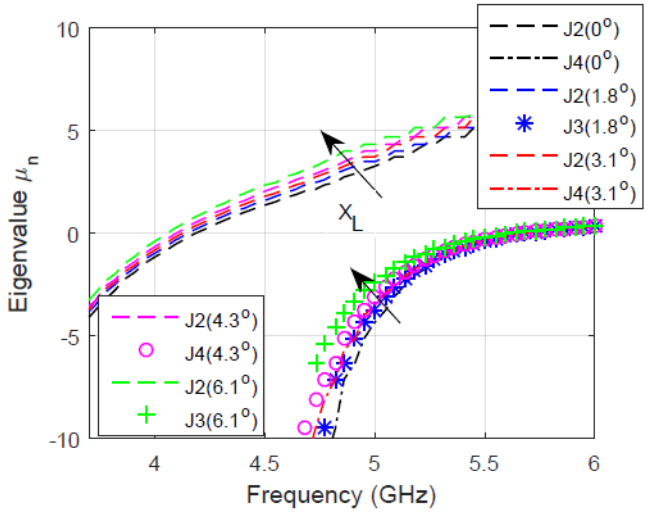

Fig. 4.11. Modal behavior of U-Slot for outer arm angle variation

4.5 Influence of Characteristics Mode on Feed Placement

The total current distribution on the surface of antenna can be constructed out of set of orthogonal modes [2]

$$J = \sum_n \alpha_n J_n \tag{4.15}$$

where α_n is the n[th] complex weight coefficient and can be defined as

$$\alpha_n = \frac{V_n^i}{1+j\lambda_n} = \frac{\langle J_n, E^i \rangle}{1+j\lambda_n} = \frac{J_n(P)}{1+j\lambda_n} \tag{4.16}$$

which shows that _n of only few modes, which have small eigenvalues, can contribute to the total radiated field at a specific frequency [79]. V I n is the modal excitation coefficient which account for the way of position, magnitude, phase of feed effect on each mode contribution to the total current [82].

For a voltage excitation of 1 V, the input admittance of the antenna at the feeding point can be written as [80]:

$$Y_{in}[P] = \sum_n \frac{V_n^i J_n(P)}{1+j\lambda_n} \tag{4.17}$$

which can be expressed as complex admittances of each mode as:

$$\begin{aligned} Y_{in}[P] &= \sum_n^N Y_n = \sum_n^N G_n + jB_n \\ &= \sum_n \left(\frac{V_n^i J_n(P)}{1+j\lambda_n^2} - j\frac{V_n^i J_n(P)\lambda_n}{1+j\lambda_n^2}\right) \\ &= \sum_n \frac{V_n^i J_n(P)}{1+j\lambda_n^2}(1-j\lambda_n) = \sum_n \alpha_n V_n^i \end{aligned} \tag{4.18}$$

where input admittance is the sum of modal admittances.

Modal admittance is composed of modal conductance G and suceptance B. Modal currents ‘Jn’ and admittance are the function of feed point (P) position. Feed location can optimize modal currents for desired performance. The new eigen value _ after optimizing feed position can be written as [88]

$$\mu_n = \frac{B_n}{G_n}$$

(4.19)

Feed location or feed point placement can control the eigen values of the contributing modes. Probe feed adds a reactive load in series with the overall impedance of U-Slot, as shown in Fig.4.2. To analyze the effect of feed position using characteristics modes, probe feed location of the U-Slot is varied in xp and yp direction.

4.5.1 Variation in xp direction

When feed is moved in the direction of x-axis (vertical currents), impedance loop got big and shifted to capacitive region as shown in smith chart plot in Fig.4.12 . It can be seen in return loss plot in Fig.4.13 that as feed is moved from (0,0) to (0.5,0) higher order resonant frequency is increased from 5.5 GHz to 6 GHz and lower resonant frequency decreased from 4.18 GHz to 4.14 GHz at the cost of deterioration in the impedance matching. Further movement of feed from (0.5,0) till (3,0) shows further deterioration in impedance matching and significant increase in higher order resonant frequency [20].

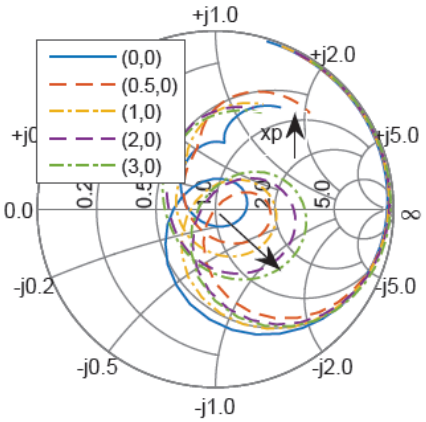

Fig. 4.12. Smit chart of U-Slot for feed location variation in xp direction. (xp,yp) values are in mm.

Eigen values of higher order modes decreases due to capacitive loading as described in (3). Modal analysis of xp feed variation in Fig.4.14 shows that eigen value of participating higher order current mode is decreased with feed variation in xp direction. J4 for (0,0) shows resonance at 5.5 GHz while resonant frequency of J4 for (3.,0) is significantly increased to 6.5 GHz. There is some decrease in lower order participating modes i.e _n = 0 for J2 (0,0) at 4.18 GHz while it is decreased to 4.14 GHz for J2(0.5,0). But overall change in higher order mode is more significant than lower order one which can also be noticed in return loss plot in Fig.13. So, the over all impedance loop shows capacitive effect. In Fig.13, it can also be noticed that lower and higher order modes are getting far from each other with xp variation, which makes it difficult for them to contribute simultaneously in impedance bandwidth for wide band behavior. Hence, the feed movement in xp direction introduces capacitive effect and increases resonant frequency of higher order modes without significantly affecting lower resonant frequency.

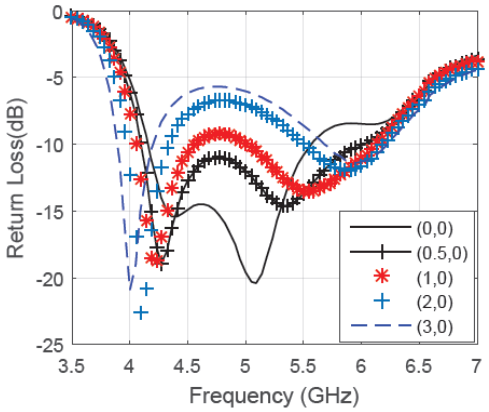

Fig.4.13.Return loss of U-Slot for feed location variation in xp direction. (xp,yp) values are in mm

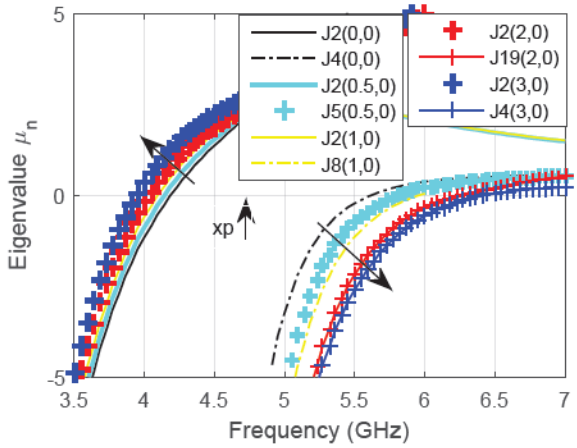

Fig.4.14. Eigenvalue behavior for feed location variation in xp direction. (xp,yp) values are in mm

4.5.2. Variation in y_p direction

Feed variation in the direction of y-axis (horizontal currents) adds an inductive reactance in over all antenna impedance as shown in Fig. 4.15. It can be noticed that for yp=0.5mm and yp=1mm change is not significant but for yp=2mm and yp=3mm significant shift to the inductive region is observed. Feed movement from (0,0) to (0,0.5) is shown to reduce the impedance matching of higher order resonant frequency with slight change in the impedance bandwidth as shown in Fig. 4.16. Further movement of feed from (0,0.5) to (0,3) shows decrease in impedance bandwidth and impedance matching.

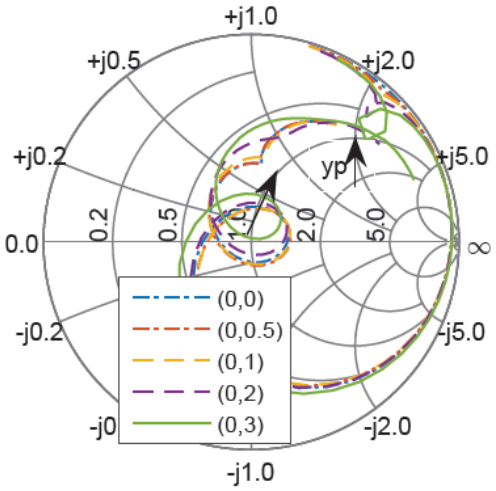

Fig. 4.15.Smithchart for feed location variation in yp direction. (xp,yp) values are in mm

yp variation (inductive) is shown to increases the eigen value of higher order modes as shown in Fig. 4.17 which decreases the higher order resonant frequency. _n = 0 for J4 (0,0) at 5.5 GHz which is reduced to 5.14 GHz for higher order mode for (0,3). This reduction in higher order resonant frequency and no variation in lower order resonant frequency brought modes closer to each other. So, their over all impedance bandwidth is reduced.

Inductive and capacitive reactance due to feed location variation changes the eigen values of participating current mode which in turn helps in optimizing the antenna. However, these results of feed variation may vary with electric thickness specially for thicker substrates where surface waves become significant to contribute in impedance matching.

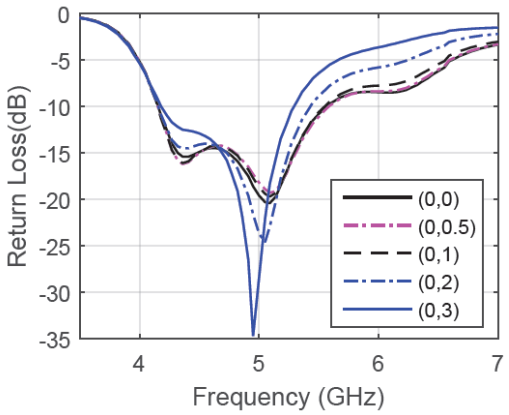

Fig. 4.16. Return loss of U-Slot for feed location variation in yp direction. (xp,yp) values are in mm

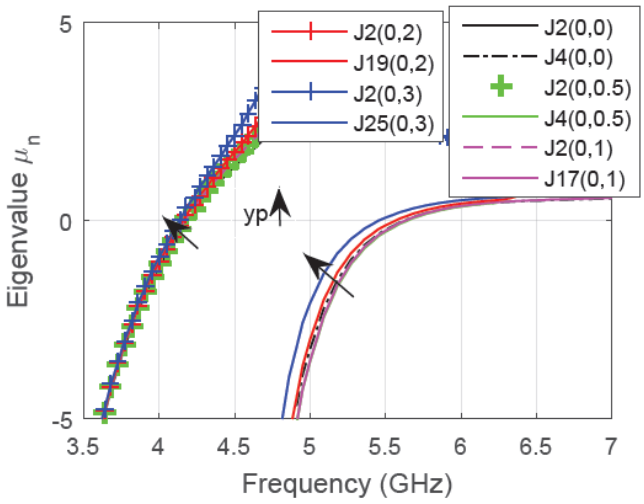

Fig 4.17. Eigenvalue behavior of U-Slot for feed location variation in yp direction. (xp,yp) values are in mm

4.6. Use of Reactive Loading Technique in Broadening Bandwidth

The concept of reactive loading due to feed and arm angle, presented in the previous sections, allows to control the eigenvalue behavior and the resonance frequency

of the respective characteristic modes. It also allows us to control the impedance loop in the smith chart. In this section, we will show by an example ,how the reactive loading concept can be applied to optimize the poorly matched U-Slot antenna.

Design Example:

1. To explain design procedure let's take an example of poorly matched U-Slot antenna. e.g A U-Slot antenna (_ = 0o) is designed and fabricated on ϵ_r = 4:4 and h=11.1811mm (h p(_r) _ =0.208) [17].
2. Impedance bandwidth of antenna is 16% because of poor impedance matching as shown in Fig.4.20. Smith chart in Fig.4.18 shows dominant capacitive effect for _ = 0o. J2 and J3 are significant participating modes for this U-Slot , shown in Fig.4.19
3. The capacitive affect can be nullified by applying inductive loading i.e. increasing outer arm angle as shown in Fig.4.9 Hence, increase in outer arm angle from _2 = 0o to _2 = 6:71o moved impedance loop up and decreases the resonant frequency for J2 than J3 as shown in Fig. 19. The inductive loading effect is more prominent on J2 than J3, thats why return loss shows shift in lower resonant frequency in Fig. 4.20.
4. Further increase in outer arm angle till _2 = 14:8o showed more decrease in resonant frequency of J2 and J3. It can be seen in Fig.4.18 that inductive loading moved the impedance loop almost in the middle but return loss plot in Fig.4.20 still shows impedance mismatching for middle frequencies for broad bandwidth. Smith chart in Fig.4.18 shows some capacitive effect as well.

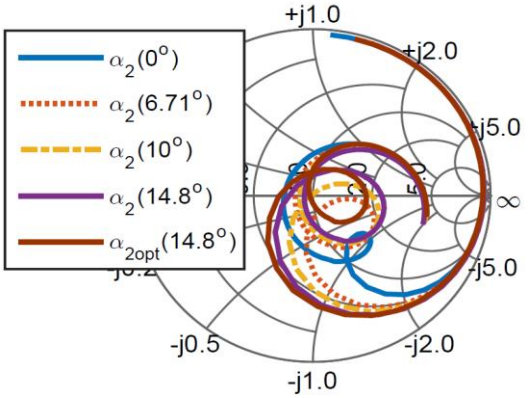

Fig 4.18. Impedance matching of U-Slot on ϵ_r= 4.4, h=11.811mm

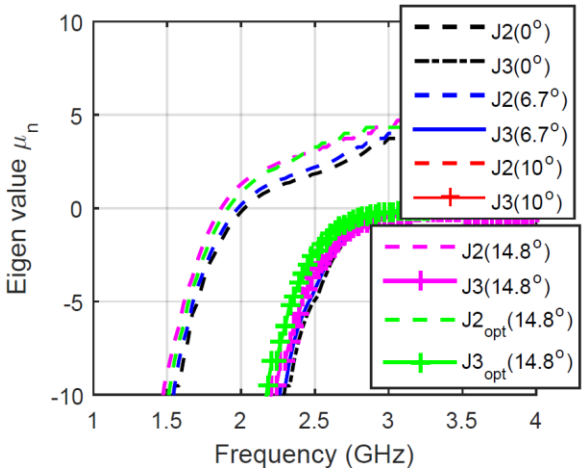

Fig 4.19. Eigenvalue behavior of U-Slot on ϵ_r = 4.4, h=11.811mm

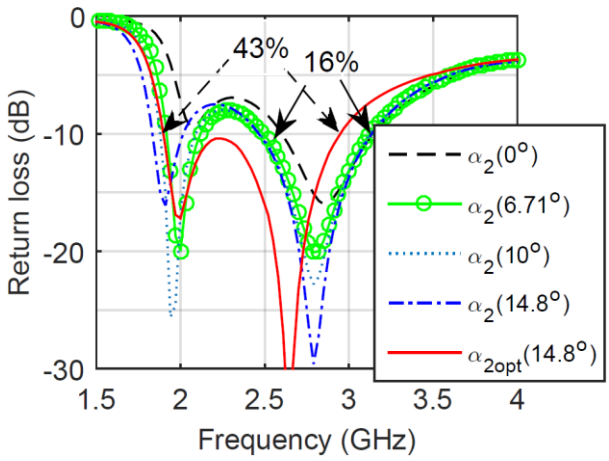

Fig 4.20. Return loss of U-Slot on ϵ_r = 4.4, h=11.811mm

5. Now the feed position is varied to decrease some capacitive loading in the design. As, the original feed position was (xp=5.1, yp=0). Based on the results of previous section, It was anticipated that decrease in xp value should improve the results. Hence, the feed position is optimized from its original position (xp=5.1, yp=0) [17] to (xp=2.5, yp=0). Interestingly, it is observed that J2's resonant frequency decreases and J3's increases due to xp variation. Now the modes are close enough to participate simultaneously for broad bandwidth.
6. Impedance bandwidth is increased from 16% to 43% as shown in Fig.4.20.
7. It is important to investigate the radiation pattern to fully understand the effect of arm- angle and feed variation on U-Slot. Radiation pattern plots for the design example are shown in Fig.21 and Fig.22. It can be seen in Fig.21 that radiation patterns maintain their shape at center frequency for all arm angles. Stable radiation pattern plots show that arm-angle variation has minimal effect on radiation pattern. Very little change in E_ is observed due to feed variation i.e. _2opt = 14:8o at _ = 0o (Fig.4.21(a)).
8. Fig.22 illustrates the modal radiation pattern of the loaded antenna for optimized arm angle i.e. _2opt = 14.8^o at different frequency points in the operating frequency range. Modal Radiation pattern are investigated for participating current modes (J2 and J3). It can be seen in Fig. that

E_ in J2 is significant at _ = 00 for all frequencies. At higher frequencies, the radiation pattern is modified due to the contribution of the ground plane. E_ have low cross polarization at all frequency points.

As, reactive loading doesnot affect radiation pattern significantly but it affects the impedance behavior. So, we have developed an optimization guideline based on the change in impedance behavior due to reactive loading of U-Slot i.e feed and arm angle variation. In the first phase, arm angle will be adjusted to move the impedance loop in the middle and then feed location variation can be used to further improve the matching of the antenna. A flowchart detailing the process is shown in Fig.4.23. Moreover, it is important to analyze the reactive loading of U- Slot on different dielectric thicknesses to improve the optimization guideline in future.

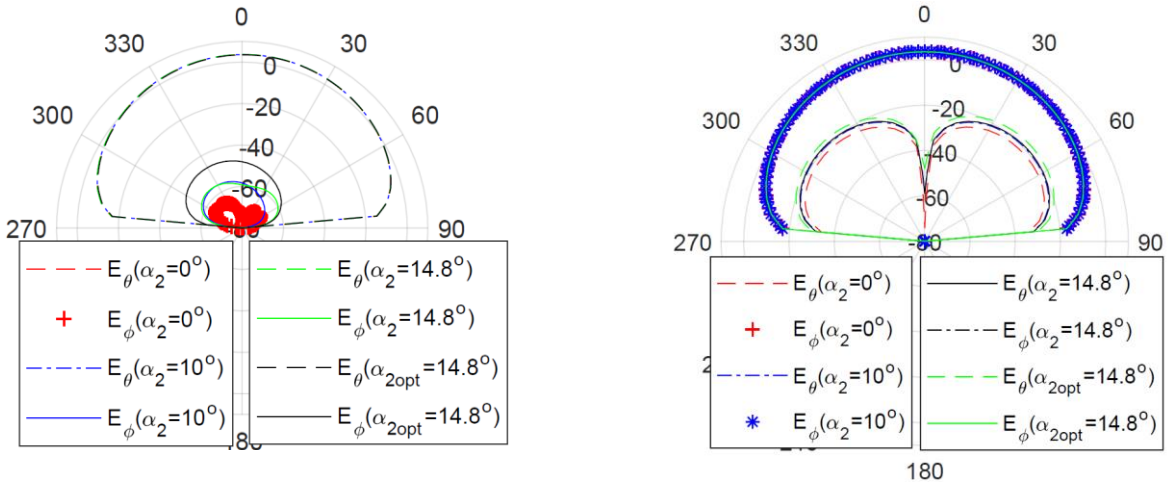

Fig 4.21. Radiation pattern of U-Slot on ϵ_r= 4.4, h=11.811mm at center frequency for (a) ϕ= 0º (b) ϕ = 90º

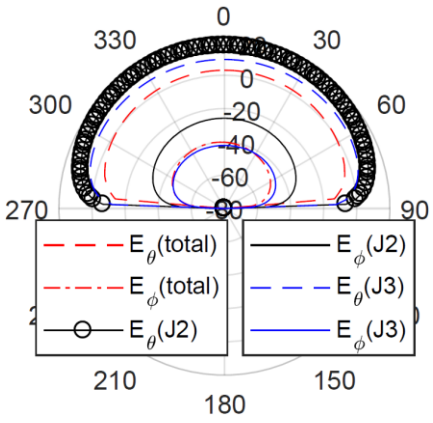

(a) Ø =0° @1.9 GHz

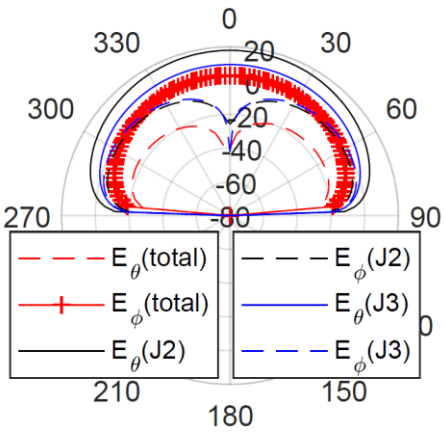

(b) Ø =90° @1.9 GHz

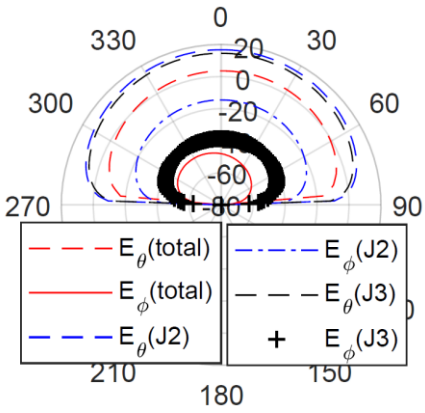

(c) Ø =0° @2.3 GHz

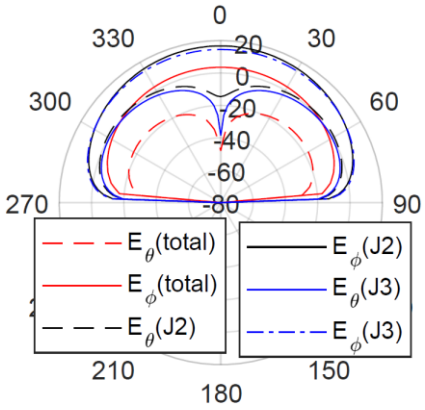

(d) Ø =90° @2.3 GHz

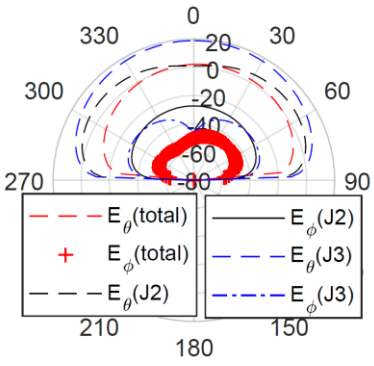

(e) Ø =0° @2.93 GHz

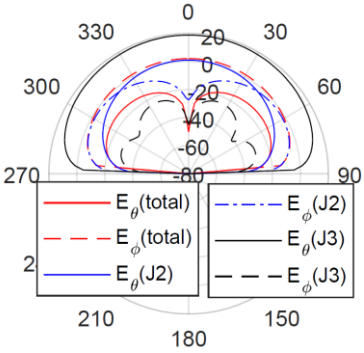

(f) Ø =90° @2.93 GHz

Fig.4.22. Modal radiation pattern of U-Slot on ϵ_r = 4.4, h=11.811mm at optimized arm-angle (_2opt = 14:8o)

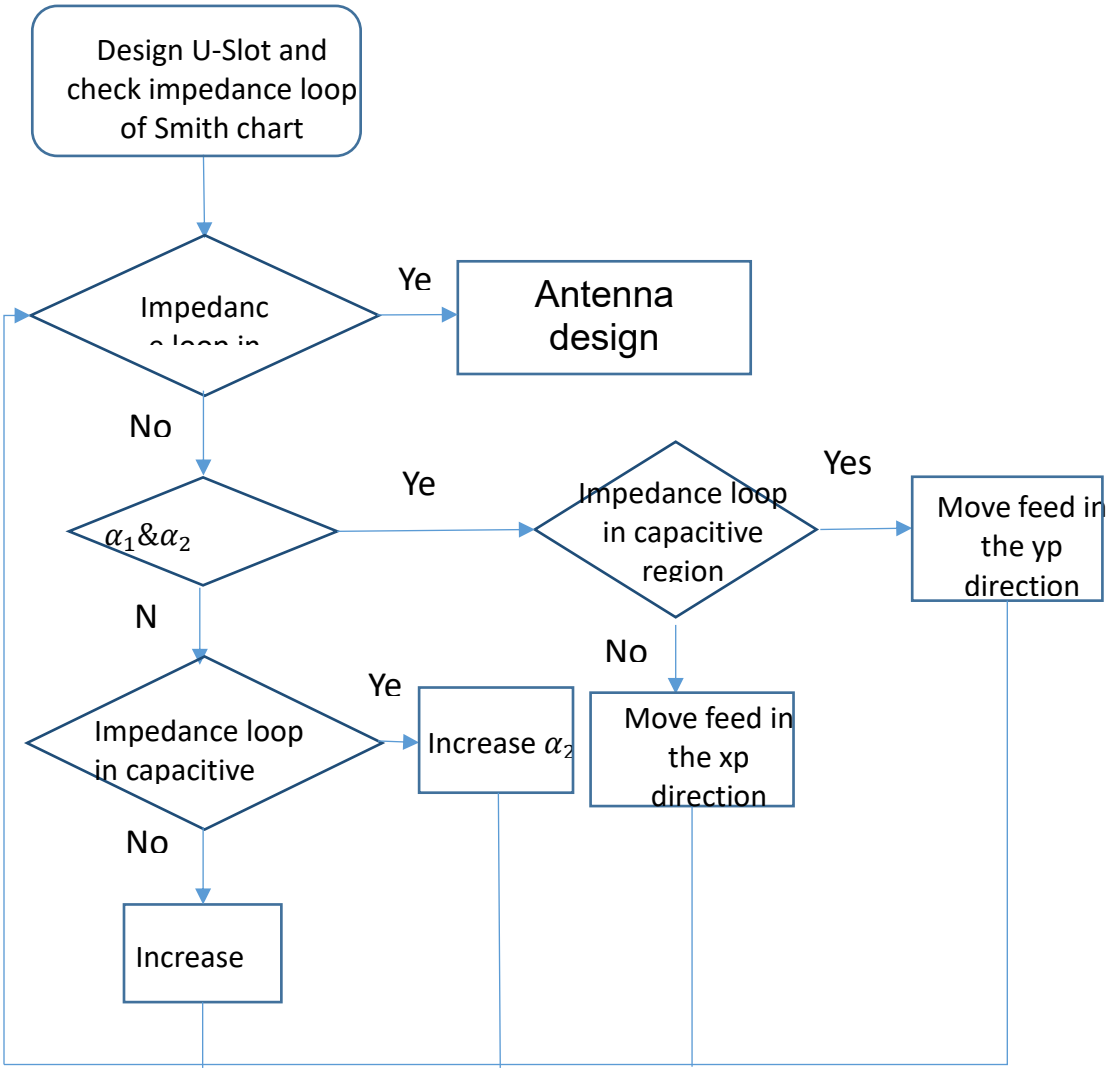

Fig .4.23. Design Procedure for optimized U-Slot structure

4.7 Summary

In this chapter, TCM analysis of U-Slot's reactive loadings due to feed placements and slot perturbations is presented. The capacitive and inductive nature of the reactive load increases or decreases the eigen value of the participating mode. The slot perturbations with unequal inner and outer arm-angle variations are shown to change the eigen value of CMs without adding any complexity in the antenna. Reactive loading due to feed location variation in the xp and yp direction can decrease or increase the eigen value respectively. Based on this information, impedance loop in smith chart has been controlled for broad bandwidth. A new optimization procedure is presented to improve input impedance matching of U-Slot. This novel optimization procedure has been shown to optimize and broaden the bandwidth of poorly matched U-Slot. It has also been shown that reactive loading has minimal effect on the far field characteristics of antenna.

CHAPTER 5

CONCLUSION AND FUTURE WORK

In this dissertation, a new empirical design method ”dimensionally invariant resonant frequency (DIResF)” for probe-fed U-Slot microstrip patch is proposed that combines the features of existing design methods i.e. dimensional invariance (DI) and resonant frequency (ResF) in such a mananer that optimum design can be achieved with minimum optimization of probe location. Performance analysis on different substrates reveal that ResF method works well for low-permittivity and electrically thin substrates while the DI method works for a much wider range of substrates that are rather arbitrary compared to ResF. Further analysis of these methods based on (fullwave) characteristic mode analysis (CMA) was carried out with the motivation to understand the modal contributions for achieving wideband designs. CMA for U-slot designs on various dielectric thicknesses indicated that current modes of DI tend to resonate at higher frequencies than ResF. This difference in modal nature is effectively exploited in DIResF technique because it combines the ResF behavior at lower frequency mode and follow DI pattern at higher order mode to provide highest 10dB return loss bandwidth. Modal analysis of probe location reveals that optimization in the direction of vertical or horizontal current modes for DI or ResF increase bandwidth but it affects polarization purity while DIResF mostly needs no probe location optimization for bandwidth enhancements. CM analysis of probe radius suggests that increase in probe radius excites higher order modes, which led to increase in bandwidth if matching is appropriate.

Two immediate future tasks are identified, as below:

(1) Though the parametric study for the characteristic modes has been reported here,i.e., for electrical thickness, probe radius and location, slot thickness variations, the property of dimensional invariance for U-Slot, as reported in [16] and shown in Table I, is not fully understood.Segmentation analysis as proposed in [17] and [18] can be useful for this investigation in future. However one major drawback in [17],[18] is that the surface wave power is ignored through the thin substrate assumption. This needs to be carefully incorporated in the analysis.

(2) The CM analysis in FEKO[37] uses the free-space Green's function which is the most suitable for microstrip patch antennas on small, finite ground planes. However extensive computational resources are required for electrically large ground plane. In such situations an alternative would be to use the infinite ground plane approximation, where the Green's function now contains Sommerfeld integrals[35]. The influence of the finite ground size on approach as an alternative to the method described in [45]. Finally, it is worth mentioning that a relationship between CMs, optimal currents and antenna Q, following the recent work in [43],[42] may perhaps be a worthy investigation too.

APPENDIX A

A. MATLAB CODE

This appendix presents the MATLAB code used to calculate the dimensions of the

U-slot rectangular microstrip patch antenna using the method of dimensional invariance.

Also, the MATLAB code used to calculate the antenna's fidelity in section 2.3 is presented.

Finally, the MATLAB code used to calculate the nonuniform element spacing in the 17-

element linear array in section 4.2 is presented.

A.1. MATLAB Code for the Method of Dimensional Invariance [41]

```
%%%%Input Parameters%%%%%
eps_r = 4.4;                    % substrate permittivity
f_r = 8.0*(10^9);               % design frequency
h = 1.0;                        % substrate thickness
pi = 3.14159;
c = 2.99*10^11;
f_r0 = (1.25*f_r);
lam = c/f_r;
C = h/lam;
L = c/(2*f_r0*sqrt(eps_r));     % rectangular patch length
W = 1.385*L;                    % rectangular patch width
W_out = ((eps_r + 1)/2)+((eps_r -
1)/(2*sqrt(1+(10*h/W)))); L_out = ((eps_r + 1)/2)+((eps_r
- 1)/(2*sqrt(1+(10*h/L))));
del_L = ((0.412*h)*(W_out+0.3)*((W/h) + 0.264))/((W_out-0.258)*((W/h)+0.8));
f_H = c/(2*(L+del_L)*sqrt(eps_r))
x = ((h/L)*(0.882+(0.164*(eps_r-
1)/(eps_r*eps_r))))+(((eps_r+1)/(pi*eps_r))*(0.758+log(1.88+L/h))
); f_J = (f_r0*eps_r)/((1+x)*sqrt(W_out*L_out))
```

```
% Calculation of the upper and lower limits of the design
frequency while ((f_r >= min(f_H,f_J)) && (f_r <=
max(f_H,f_J))) == 0
    fprintf('entered
    while\n'); if f_r <
    min(f_H,f_J)
        fprintf('entered f_r <
        min(f_H,f_J)'); f_r0 = f_r0-
        (0.05*f_r);
        L =
        c/(2*f_r0*sqrt(eps_r));
        W = 1.385*L;
        W_out = ((eps_r + 1)/2)+((eps_r -
        1)/(2*sqrt(1+(10*h/W)))); L_out = ((eps_r + 1)/2)+((eps_r
        - 1)/(2*sqrt(1+(10*h/L))));

        del_L = ((0.412*h)*(W_out+0.3)*((W/h) + 0.264))/((W_out-0.258)*((W/h)+0.8));
        f_H = c/(2*(L+del_L)*sqrt(eps_r))
        x = ((h/L)*(0.882+(0.164*(eps_r-
1)/(eps_r*eps_r))))+(((eps_r+1)/(pi*eps_r))*(0.758+log(1.88+L/h)));
        f_J = (f_r0*eps_r)/((1+x)*sqrt(W_out*L_out))
    elseif (f_r > max(f_H,f_J))
        fprintf('entered f_r > max(f_H,f_J)');
        f_r0 = f_r0+(0.05*f_r);
        L =
        c/(2*f_r0*sqrt(eps_r));
        W = 1.385*L;
        W_out = ((eps_r + 1)/2)+((eps_r -
        1)/(2*sqrt(1+(10*h/W)))); L_out = ((eps_r + 1)/2)+((eps_r
        - 1)/(2*sqrt(1+(10*h/L))));
        del_L = ((0.412*h)*(W_out+0.3)*((W/h) + 0.264))/((W_out-
        0.258)*((W/h)+0.8)); f_H = c/(2*(L+del_L)*sqrt(eps_r))
        x = ((h/L)*(0.882+(0.164*(eps_r-
1)/(eps_r*eps_r))))+(((eps_r+1)/(pi*eps_r))*(0.758+log(1.88+L/h))
        ); f_J = (f_r0*eps_r)/((1+x)*sqrt(W_out*L_out))
    end
end
L_1= L;

%%%%%%%%%% Dimensions of the U-slot %%%%%%%%%%
if eps_r <= 1
    W_s = W/3.203;
    L_s = W_s/0.835;
    t =
    W_s*0.13;
```

```
    b           =
    L_s/4.237;
elseif eps_r > 1 && eps_r <= 3
    W_s = W/2.573;
    L_s = W_s/0.777;
    t =
    W_s*0.144;
    b =
    L_s/4.5;
elseif eps_r > 3 && eps_r <= 5
    W_s = W/2.573;
    L_s = W_s/0.776;
    t =
    W_s*0.144;
    b =
    L_s/4.51;
else
    W_s = W/2.574;
    L_s = W_s/0.777;
    t =
    W_s*0.144;
    b =
    L_s/4.48;
end
F = L/2;
```

A.2 MATLAB Code for Cross-correlation Calculation of Pulse Signals

```
% The cross-correlation of the pulse signals to evaluate the antenna
fidelity resp = resp_theta_45_phi_90;

pulse2 = pulse/sqrt(sum(pulse.^2));
resp2 = resp/sqrt(sum(resp.^2));
cross_corr = xcorr(pulse2,resp2);


disp('cross_corr ='); disp(cross_corr);
disp('max ='); disp(max(cross_corr));

figure (1); plot (pulse);
figure (2); plot (resp);
figure (3); plot (cross_corr);
```

A.3 MATLAB Code for Nonuniform Element Spacing Calculation

main.m:

```
N = 24;                 % number of elements
K = 4;                  % number of sidelobes reduced
A = 0.00786;            % amount of reduction        A=0.00786 for 24-element (-42dB)

for n=1:2:N-1
  eta_n = 2*A*((N/pi)^3)*sll_summ(n, K, N);
  disp('eta'); disp(n); disp(eta_n);
end
```

sll_summ.m:

```
function [sll_sum] = sll_summ(n, K, N)

sll_sum = 0;

for k=1:K
    a = (-1)^k;
    b = (2*k)+1;
    c = sin((n*pi)/(2*N)*b);
    d = c/(b^2);
    sll_sum = sll_sum + (a*d);
end
```

REFERENCES

[1] R. S. Kshetrimayum, “An introduction to UWB communication systems*,” IEEE Potentials*, vol. 28, no. 2, pp. 9-13, March-April, 2009.

[2] S. H. Choi, J. K. Park, S. K. Kim, and J. Y. Park , “A new ultra-wideband antenna for UWB applications*,” Microwave and Optical Technology Letters*, vol. 40, no. 5, pp. 399-401, March 5, 2004.

[3] L. Guo, S. Wang, X. Chen, and C. G. Parini, “Study of compact antenna for UWB applications,” *Electronics Letters*, vol. 46, no. 2, pp. 115-116, January 21, 2010.

[4] C. Sim, W. Chung, and C. Lee, “Compact slot antenna for UWB applications,” *IEEE Antennas and Wireless Propagation Letters*, vol. 9, pp. 63-66, 2010.

[5] A. A. L. Neyestanak, “Ultra wideband rose leaf microstrip patch antenna,” *Progress In Electromagnetics Research*, vol. 86, pp. 155-168, 2008.

[6] M. N. Shakib, M. T. Islam and N. Misran, “Stacked patch antenna with folded patch feed for ultrawideband application,” *IET Microwave Antennas and Propagation*, vol. 4, no. 10, pp. 1456-1461, 2010.

[7] R. Zaker and A. Abdipour, "A very compact ultrawideband printed omnidirectional monopole antenna,” *IEEE Antenna and Wireless Propagation Letters*, vol. 9, pp. 471-473, June 2010.

[8] Q. Wu, R. Jin, J. Geng, and M. Ding, “Printed omni-directional UWB monopole antenna with very compact size,” *IEEE Transactions on Antennas and Propagation*, vol. 56, no. 3, pp. 896–899, Mar. 2008.

[9] J. Jung, W. Choi, and J. Choi, "A small wideband microstrip-fed monopole antenna,"*IEEE Microwave Wireless Components Letters*, vol. 15, no. 10, pp. 703–705, Oct. 2005.

[10] R. Azim, M.T. Islam, and N. Misran, "Compact tapered-shape slot antenna for UWB applications," *IEEE Antennas Wireless Propagation Letters*, vol. 10, pp. 1190–1193, 2011.

[11] N. Chahat, M. Zhadobov, R. Sauleau, and K. Ito, "A compact UWB antenna for on-body applications," *IEEE Transactions on Antennas and Propagation*, vol. 59, no. 4, pp. 1123–1131, April 2011.

[12] S. A. Hosseini, Z. Atlasbaf, and K. Forooraghi, "A compact ultra wide band (UWB) planar antenna using glass as substrate," *Journal of Electromagnetic Waves and Applications*, vol. 22, no. 1, pp. 47 59, Jan. 2008.

[13] G. A. Deschamps, "Microstrip microwave antennas," *Proc. 3rd USAF Symposium on Antennas*, 1953.

[14] R. E. Munson, "Conformal microstrip antennas and microstrip phased arrays," *IEEE Transactions on Antennas and Propagation*, vol. AP-22, pp. 74-78, 1974.

[15] J. Q. Howell, "Microstrip antennas," *IEEE Transactions on Antennas and Propagation*, vol. AP-23, pp. 90-93, January 1975.

[16] R. Garg, P. Bhartia, I. Bahl, A. Ittipiboon, *Microstrip Antenna Design Handbook*, Artech House, Norwood, MA, 2001.

[17] D. Gibbins, M. Klemm, I.J. Craddock, J.A. Leendertz, A. Preece, and R. Benjamin, "A comparison of a wide-slot and a stacked patch antenna for the purpose of breast cancer detection," *IEEE Transactions on Antennas and Propagation*, vol. 58, no. 3, pp. 665-674, March 2010.

[18] M. Bassi, M. Caruso, M.S. Khan, A. Bevilacqua, A.D. Capobianco, and A. Neviani,, "An integrated microwave imaging radar with planar antennas for breast cancer detection," *IEEE Transactions on Microwave Theory and Techniques*, vol. 61, no. 5, pp. 2108-2118, May 2013.

[19] H. M. Jafari, W. Liu, S. Hranilovic, and M. J. Deen, "Ultrawideband radar imaging system for biomedical applications," *Journal of Vacuum Science & Technology*, vol. 24, no. 3, pp. 752-757, May 2006.

[20] W. Liu, H.M. Jafari, S. Hranilovic, and M.J. Deen, "Time domain analysis of UWB breast cancer detection," *IEEE 23rd Biennial Symposium on Communications*, pp. 336-339, 2006.

[21] X. Zhuge, M. Hajian, A. G. Yarovoy, and L. P. Ligthart, "Ultra-wideband imaging for detection of early-stage breast cancer," *IEEE Proceedings of the European Radar Conference (EuRAD)*, pp. 39-42, October 10-12, 2007.

[22] E. C. Fear and M. A. Stuchly, "Microwave detection of breast cancer: a study of tumor response variations," *IEEE Proceedings of the 22nd Annual International Conference in Engineering in Medicine and Biology Society (EMBS)*, pp. 74-77, July 23-28, 2000.

[23] S. Adnan, "A compact UWB antenna design for breast cancer detection," *PIERS Online*, vol. 6, no. 2, pp. 129-132, 2010.

[24] R. Nilavalan, I.J. Craddock, A. Preece, J. Leendertz and R. Benjamin, "Wideband microstrip patch antenna design for breast cancer tumour detection," *IET Microwave Antennas Propagation*, vol. 1, no. 2, pp. 277-281, 2007.

[25] H. Kanj and M. Popovic, "A novel ultra-compact broadband antenna for microwave breast tumor detection," *Progress In Electromagnetics Research (PIER) vol. 86, pp. 169–198, 2008.*

[26] X. Chen, J. Liang, S. Wang, Z. Wang and C. Parini, "Small ultra wideband antennas for medical imaging," *2008 Loughborough Antennas & Propagation Conference*, pp. 28-31, 17-18 March 2008.

[27] G. Kumar and K. P. Ray, *Broadband Microstrip Antennas,* Artech House, Norwood, MA, 2003.

[28] R. Garbacz, "Modal Expansions for Resonance Scattering Phenomena," *Proceedings of the IEEE*, pp. 856 – 864, August 1965.

[29] R. Garbacz, R. Turpin, "A Generalized Expansion for Radiated and Scattered Fields", *IEEE Transactions on Antennas and Propagation*, Vol. AP-19, No. 3, May 1971.

[30] R.F. Harrington, J Mautz, "Theory of Characteristic Modes for Conducting Bodies*", IEEE Transactions on Antennas and Propagation*, Vol. AP-19, No. 5, Sept 1971.

[31] R. F. Harrington, J. Mautz, *"*Computation of Characteristic Modes for Conducting Bodies", *IEEE Transactions on Antennas and Propagation*, Vol. AP-19, No. 5, pp. 629 – 639, September 1971.

[32] H. Huynh and K.-F. Lee, "Single-layer single-patch wideband microstrip antenna," *Electron. Lett.*, vol. 31, no. 16, pp. 1310–1312, Aug. 1995.

[33] K.-F. Tong, K.-M. Luk, K.-F. Lee, and R. Q. Lee, "A broad-band U-slot rectangular patch antenna on a microwave substrate," *IEEE Trans. Antennas Propag.*, vol. 48, no. 6, pp. 954–960, Jun. 2000.

[34] K. F. Lee, S. L. S. Yang, A. A. Kishk, and K. M. Luk, "The versatile U-slot patch antenna," *IEEE Antennas Propag. Mag.*, vol. 52, no. 1, pp. 71–88, Feb. 2010

[35] M. Clenet and L. Shafai, "Multiple resonances and polarisation of U-slot patch antenna," *Electron. Lett.*, vol. 35, no. 2, pp. 101–103, Jan. 1999.

[36] M. Koohestani and M. Golpour, “U-shaped microstrip patch antenna with novel parasitic tuning stubs for ultra wideband applications,” *IET Microw. Antennas Propag.*, vol. 4, no. 7, pp. 938–946, 2010.

[37] G. F. Khodae, J. Nourinia, and C. Ghobadi, “A practical miniaturize U-slot patch antenna with enhanced bandwidth,” *Prog. Electromagn. Res. B*, vol. 3, pp. 47–62, 2008.

[38] J. Córcoles, M. A. González, J. Rubio, and J. Zapata, “Performance characterization of wideband, wide-angle scan arrays of cavity-backed U-slot microstrip patch antennas,” *Int. J. RF Microw. Comput.-Aided Eng.*, vol. 19, no. 3, pp. 389–396, Dec. 2008.

[39] H. Wang, X. B. Huang, and D. G. Fang, “A single layer wideband U-slot microstrip patch antenna array,” *IEEE Antennas Wireless Propag. Lett.*, vol. 7, pp. 9–12, Feb. 2008.

[40] R. Garg, P. Bhartia, I. Bahl, and A. Ittipiboon, *Microstrip Antenna Design Handbook*. Boston, MA, USA: Artech House, 2001.

[41] K.F. Lee and K. M. Luk, *Microstrip Patch Antennas*. London, U.K.: Imperial College Press, 2011.

[42] S. Bhardwaj and Y. Rahmat-Samii, “A comparative study of C-shaped,E-shaped, and U-slotted patch antennas,” *Microw. Opt. Technol. Lett.*, vol. 54, no. 7, pp. 1746–1757, Jul. 2012.

[43] J. A. Ansari and B. R. Ram, “Analysis of broad band U-slot microstrip patch antenna,” *Microw. Opt. Technol. Lett.*, vol. 50, no. 4, pp. 1069–1073, Apr. 2008.

[44] A. A. Deshmukh and K. P. Ray, “Analysis of broadband variations of U-slot cut rectangular microstrip antennas,” *IEEE Antennas Propag. Mag.*, vol. 57, no. 2, pp. 181–193, Apr. 2015.

[45] S. Costanzo and A. Costanzo, “Compact MUSA: Modified U-slot patch antennas with reduced cross-polarization,” *IEEE Antennas Propag.Mag.*, vol. 57, no. 3, pp. 71–80, Jun. 2015.

[46] S. Weigand, G. H. Huff, K. H. Pan, and J. T. Bernhard, “Analysis and design of broad-band single-layer rectangular U-slot microstrip patch antennas,” *IEEE Trans. Antennas Propag.*, vol. 51, no. 3, pp. 457–468, Mar. 2003.

[47] V. Natarajan and D. Chatterjee, “An empirical approach for design of wideband, probe-fed, U-slot microstrip patch antennas on single-layer, infinite, grounded substrates,” *ACES J.*, vol. 18, no. 3, pp. 191–200, Nov. 2003.

[48] E. G. Lim, E. Korolkiewicz, S. Scott, B. Aljibouri, and S.-C. Gao, “Efficient impedance coupling formulas for rectangular segment in planar microstrip circuits,” *IEEE Trans. Antennas Propag.*, vol. 51, no. 8, pp. 2137–2140, Aug. 2003.

[49] S. K. Lee, S. F. Ooi, A. Sambell, E. Korolkiewicz, and S. Scott, “Application of segmentation analysis to a matched U-slot patch antenna,” *Microw. Opt. Technol. Lett.*, vol. 50, no. 10, pp. 2608–2611, Oct. 2008.

[50] J. Chalas, K. Sertel, and J. L. Volakis, “Computation of the *Q* limits for arbitrary-shaped antennas using characteristic modes,” in *Proc. IEEEInt. Symp. Antennas Propag.*, Jul. 2011, pp. 772–774.

[51] G. Angiulli, G. Amendola, and G. Di Massa, “Application of characteristic modes to the analysis of scattering from microstrip antennas,” *J. Electromagn. Waves Appl.*, vol. 14, no. 8, pp. 1063–1081,

[52] Y. Chen and C.-F. Wang, “Characteristic-mode-based improvement of circularly polarized U-slot and E-shaped patch antennas,” IEEE Antennas Propag. Lett., vol. 11, pp. 1474–1477, Nov. 2012.

[53] E. Antonino-Daviu, M. Fabres, M. Ferrando-Bataller, andV. M. R. Penarrocha, “Modal analysis and design of band-notched UWB planar monopole antennas,” IEEE Trans. Antennas Propag., vol. 58, no. 5, pp. 1457–1467, May 2010.

[54] M. Cabedo-Fabres, E. Antonino-Daviu, A. Valero-Nogueira, and M. F. Bataller, “The theory of characteristic modes revisited: A contribution to the design of antennas for modern applications,” IEEE Antennas Propag. Mag., vol. 49, no. 5, pp. 52–68, Oct. 2007.

[55] N. L. Bohannon and J. T. Bernhard, “Design guidelines using characteristic mode theory for improving the bandwidth of PIFAs,” IEEE Trans. Antennas Propag., vol. 63, no. 2, pp. 459–465, Feb. 2015.

[56] J. J. Adams and J. T. Bernhard, “Broadband equivalent circuit models for antenna impedances and fields using characteristic modes,” IEEE Trans. Antennas Propag., vol. 61, no. 8, pp. 3985–3994, Aug. 2013.

[57] E. H. Newman, “Small antenna location synthesis using characteristic modes,” IEEE Trans. Antennas Propag., vol. 27, no. 4, pp. 530–531, Jul. 1979.

[58] R. F. Harrington, Field Computation by Moment Methods. New York, NY, USA: IEEE Press, 1993.

[59] R. F. Harrington, Time-Harmonic Electromagnetic Fields. New York, NY, USA: McGraw-Hill, 1961.

[60] Y. Chen and C.-F.Wang, Characteristic Modes: Theory and Applications in Antenna Engineering. Hoboken, NJ, USA: Wiley, 2015.

[61] Q. I. Dai, Q. S. Liu, H. U. I. Gan, and W. C. Chew, “Combined field integral equation-based theory of characteristic mode,” IEEE Trans. Antennas Propag., vol. 63, no. 9, pp. 3973–3981, Sep. 2015.

[62] Q. I. Dai, J. Wu, H. U. I. Gan, Q. S. Liu, W. C. Chew, and W. E. I. Sha, “Large scale characteristic mode analysis with fast multipole algorithms,” IEEE Trans. Antennas. Propag.,

[63] .E. H. Newman, “An overview of the hybrid MM/Green’s function method in electromagnetics,” Proc. IEEE, vol. 76, no. 3, pp. 270–282, Mar. 1988.

[64] K. A. Michalski and J. R. Mosig, “Multilayered media Green’s functions in integral equation formulations,” IEEE Trans. Antennas Propag., vol. 45, no. 3, pp. 508–519, Mar. 1997.

[65] A. Z. Elsherbeni, P. Nayeri, and C. J. Reddy, Antenna Analysis and Design Using FEKO Electromagnetic Simulation Software. Edison, NJ, USA: SciTech, 2014.

[66] B. D. Raines, “Systematic design of multiple antenna systems using characteristic modes,” Ph.D. dissertation, Dept. Elect. Comput. Eng., Ohio State Univ., Columbus, OH, USA, 2011.

[67] M. Capek, P. Hamouz, P. Hazdra, and J. Eichler, “Implementation of the theory of characteristic modes in MATLAB,” IEEE Antennas Propag.Mag., vol. 55, no. 2, pp. 176–189, Apr. 2013.

[68] M. Vogel, G. Gampala, D. Ludick, U. Jakobus, and C. J. Reddy, “Characteristic mode analysis: Putting physics back into simulation,” IEEE Antennas Propag. Mag., vol. 57, no. 2, pp. 307–317, Apr. 2015.

[69] A. D. Yaghjian and S. R. Best, “Impedance, bandwidth, and Q of antennas,” IEEE Trans. Antennas Propag., vol. 53, no. 4, pp. 1298–1324, Apr. 2005.

[70] M. Gustafsson, M. Cismasu, and B. L. G. Jonsson, “Physical bounds and optimal currents on antennas,” IEEE Trans. Antennas Propag., vol. 60, no. 6, pp. 2672–2681, Jun. 2012.

[71] M. Gustafsson and S. Nordebo, “Optimal antenna currents for Q, superdirectivity, and radiation patterns using convex optimization,” IEEE Trans. Antennas Propag., vol. 61, no. 3, pp. 1109–1118, Mar. 2013.

[72] E. Safin and D. Manteuffel, “Reconstruction of the characteristic modes on an antenna based on the radiated far field,” IEEE Trans. Antennas Propag., vol. 61, no. 6, pp. 2964–2971, Jun. 2013.

[73] S. Maci, L. Borselli, and L. Rossi, “Diffraction at the edge of a truncated grounded dielectric slab,” IEEE Trans. Antennas Propag., vol. 44, no. 6, pp. 863–873, Jun. 1996.2000.

[74] M. Fabres, E. Daviu, M. Bataller, and A. Nogueira, “On the use of characteristics modes to describe patch antenna performance.” in International Symposium on Antennas and Propagation Society, 2003, pp. 712–715.

[75] Y. Chen and C. Wang, “Charcteristic mode based improvement of circularly polarized u-slot and e-shaped patch antennas,” IEEE Antennas. Propagat. Lett., vol. 11, pp. 1474-1477, 2012.

[76] J. C. Schindler, R. B. Mack, and P. Blacksmith, Jr., “The Control of Electromagnetic Scattering by Impedance Loading,”Proc. IEEE, vol. 53, pp. 993-1004, Aug. 1965.

[77] R. F. Harrington and J. R. Mautz, Control of radar scattering by reactive loading. IEEE Trans. Antennas Propag., vol. 20, no. 4, pp. 446454, Jul.1972.

[78] E. Safin and D. Manteuffel, “Manipulation of characteristics wave modes by Impedance loading.”IEEE Trans. Antennas. Propagat., vol. 63, no. 4, pp. 1756-1764, April 2015.

[79] Matthew W. Young and Jennifer T. Bernhard, “Characteristic Mode Investigation of a Reactively Loaded Electrically Small Dipole Antenna”,2015 9th European Conference on Antennas and Propagation, EuCAP 2015,Aug 2015.

[80] E. A. Daviu and M. C. Fabres, “Modal Analysis and Design of Bandnotched UWB Planar Monopole Antennas.IEEE Trans. Antennas. Propag., vol. 58, no. 5, pp.14571467, May 2010.

[81] Shivnarayan and B.R. Vishvakarma, “Analysis of inclined slot loaded patch for dual band operation,”Microwave and Optical Technology Letters, vol. 48, no. 12, pp. 2436-2441, December 2006.

[82] J. A. Ansari and B. R. Ram, “Analysis of Broad-Band U-Slot Microstrip Patch Antenna,”Microwave and Optical Technology Letters,vol. 50, no. 4, pp. 1069–1073, 2008.

[83] Gh.Rafi and L. Shafai, “Broadband microstrip patch antenna with Vslot,” IEE Proc.-Micorw.Antennas Propag., vol. 151, no. 5, pp. 435-440, October2004.

[84] J. A. Ansari, S. K. Dubey, P. Singh, R. U. Khan and B. R. Vishvakarma,“Analysis of V-Slot loaded Patch for wideband operation,” Microwaveand Optical Technology Letters,vol. 50, no. 12, pp. 3069-3075, December 2008.

[85] M. Fabres, E. Daviu, A. Nogueria, and M. Bataller, “The theory of characteristic modes revisited: A contribution to the design of antennas for modern applications,” IEEE Antennas and Propagation Magazine, vol. 49, no. 5, pp. 52–68, October 2007.

[86] A. Z. Elsherbeni, P. Nayeri and C. J. Reddy,Antenna Analysis and Design FEKO Electromagnetic Simulation Software. NJ, USA:SciTech Publications, 2014.

[87] M. Khan and D. Chatterjee,“Characteristic Mode Analysis of a Class of Empirical Design Techniques for Probe-Fed U-Slot Microstrip Patch Antennas,” IEEE Trans.Antennas. Propagat., vol. 64, no. 7, pp.2758-2770, July,2016.

[88] B. T. Strojny,“Excitation and Analysis of Characteristic Modes on complex antenna structure,” Ph.D. dissertation, The Ohio State University,2011.

[89] E. A. Daviu, M. C. Fabres, M. Sonkki, N. M. Hicho and M. Bataller,"Design Guidelines for the Excitation of Characteristic Modes in Slotted Planar Structures." IEEE Trans. Antennas. Propagat.,vol. 64, no. 12, pp.5020-5029, Dec 2016.

[90] H. Jaafar, S. Collardey and A. Sharaiha,"Optimized Manipulation of the Network Characteristic Modes for Wideband Small Antenna Matching."IEEE Trans. Antennas. Propagat., vol. pp, no. 99, Sep 2017.

[91] W. L. Stutzman and G. A. Thiele, *Antenna Theory and Design,* 3rd Edition, Wiley, New York, 2011.

[92] Y. X. Guo, K. M. Luk and K. F. Lee, "U-slot circular patch antennas with L-probe feeding," *Electronics Letters,* vol. 35, no. 20, pp. 1694-1695, September 1999.

[93] R. Garg, *Analytical and Computational Methods in Electromagnetics,* Artech House, Norwood, MA, 2008.

[94] M. N. O. Sadiku, *Numerical Techniques in Electromagnetics with MATLAB,* 3rd Edition, CRC Press, Boca Raton, FL.

[95] M. Khan and D. Chatterjee, "Analysis of Reactive Loading in U-Slot Microstrip Patch using Theory of Characteristics Modes," Submitted for second revision in *IEEE Antennas and Propagation Magazine, 2017.*

[96] M. Khan and K. F. Warnick, "Noise Figure Reduction by Port Decoupling for a Dual Circular Polarized Microstrip Antenna", *IET Electronics Letters,* vol. 15, no. 23, pp. 1662-1664, 2014.

[97] M. Khan, Z. Yang and K. F. Warnick, "Dual Circular Polarized High Efficiency Antenna for Ku band Satellite Communication", *IEEE Antennas and Wireless Propagation Letters (AWPL),* vol. 13, pp. 1624-1627, 2014.

[98] M. Khan and D. Chatterjee, “Characteristic Modes for U-Slot’s Feed Placement” 2017 *IEEE International Symposium of Antennas and Radio wave Propagation (APS/URSI),* July 2017.

[99] M. Khan and D. Chatterjee, “Design of Miniaturized Multiple U-Slots Antenna using Theory of Characteristic Modes ” *2017 IEEE International Symposium of Antennas and Radio wave Propagation (APS/URSI),* July 2017.

[100] M. Khan and D. Chatterjee, “ Effect of Feeding Techniques on U-Slot Loaded Microstrip Patch ” *2016 IEEE International Symposium of Antennas and Radio wave Propagation (APS/URSI),* June 2016.

[101] M. Khan and D. Chatterjee, “Modal Analysis of Perturbations in U-Slot Micro-strip Patch.” *Proceedings of 2016 IEEE International Symposium on Antennas and Propagation (APS/URSI),* June2016

[102] M. Khan and D. Chatterjee, “Performance Optimization of Multiple U-Slot Antennas using Theory of Characteristic Modes” *2016 IEEE International Symposium on Phased Array Systems & Technology,* Oct 2016.

[103] M. Khan and D. Chatterjee, “UWB L-Probe Proximity Fed V-Slot Patch Antenna for Early Detection of Breast Cancer” *2015 IEEE International Symposium of Antennas and wave Propagation(APS/URSI),* July 2015.

[104] M. Khan and D. Chatterjee, “UWB Microwave Sensor Array Characterization for Early Detection of Breast Cancer” *2015 IEEE Applied Electromagnetic Conference (AEMC),* Dec 2015.

[105] S. Vemulapalli, M. Khan, and D. Chatterjee, “Analysis of Ultra-wideband Microwave Imaging via Space Time Beamforming Algorithm in the Frequency Domain,” *2015 IEEE Applied Electromagnetic Conference (AEMC)*, Dec 2015.

[106] M. Khan, “Novel S-Band Phase Modulator Using Hybrid Coupler, *2009 IEEE Asia Pacific Microwave Conference (APMC)*, Jan 2009.

VITA

Mahrukh Khan was born on June 29, 1985 in Wah Cantt, Pakistan. She received her Bachelor's degree in Electrical Engineering from the University of Engineering and Technology, Lahore in 2007. She received her Master's degree in Electrical Engineering from the same University in 2011.

Mahrukh pursued an Interdisciplinary PhD degree at the University of Missouri – Kansas City. Her primary PhD discipline is Electrical and Computer Engineering. Her co-discipline is Physics. Her research interests are in the areas of ultra-wideband microstrip patch antennas, computational Electromagnetics and slotted antennas for satellite communication and biomedical applications

Mahrukh is a member of the Institute of Electrical and Electronic Engineers (IEEE). Her research publications receives 31 citations till date. She is a reviewer of IEEE , IET journals. A list of her conference and journal publications is provided below:

Journal Publication

1. **Mahrukh Khan** and Deb Chatterjee, "Analysis of Reactive Loading in U-Slot Microstrip Patch using Theory of Characteristics Modes," Accepted in *IEEE Antennas and Propagation Magazine, 2017.*
2. **Mahrukh Khan** and Deb Chatterjee, "Characteristic Mode Analysis of a Class of Empirical Design Techniques for Probe-Fed, U-Slot Microstrip Patch Antennas," *IEEE Trans. on Antennas and Propagation.* vol. 64, no. 7, pp. 2758-2770, July 2016.
3. **Mahrukh Khan** and Karl F. Warnick, "Noise Figure Reduction by Port Decoupling for a Dual Circular Polarized Microstrip Antenna", *IET Electronics Letters,* vol. 15, no. 23, pp. 1662-1664, 2014.
4. **Mahrukh Khan,** Zhenchao Yang and Karl F. Warnick, "Dual Circular Polarized High Efficiency Antenna for Ku band Satellite Communication", *IEEE Antennas and Wireless Propagation Letters (AWPL),* vol. 13, pp. 1624-1627, 2014.

Peer reviewed Conference Proceedings

5. **Mahrukh Khan** and Deb. Chatterjee, "Characteristic Modes for U-Slot's Feed Placement" 2017 *IEEE International Symposium of Antennas and Radio wave Propagation (APS/URSI),* July 2017.
6. **Mahrukh Khan** and Deb. Chatterjee, "Design of Miniaturized Multiple U-Slots Antenna using Theory of Characteristic Modes " *2017 IEEE International Symposium of Antennas and Radio wave Propagation (APS/URSI),* July 2017.

7. **Mahrukh Khan** and Deb. Chatterjee, " Effect of Feeding Techniques on U-Slot Loaded Microstrip Patch " *2016 IEEE International Symposium of Antennas and Radio wave Propagation (APS/URSI),* June 2016.
8. **Mahrukh Khan** and Deb Chatterjee, "Modal Analysis of Perturbations in U-Slot Micro-strip Patch." *Proceedings of 2016 IEEE International Symposium on Antennas and Propagation (APS/URSI),* June2016

9. **Mahrukh Khan** and Deb Chatterjee, "Performance Optimization of Multiple U-Slot Antennas using Theory of Characteristic Modes" *2016 IEEE International Symposium on Phased Array Systems & Technology,* Oct 2016.
10. **Mahrukh Khan** and Deb Chatterjee, "UWB L-Probe Proximity Fed V-Slot Patch Antenna for Early Detection of Breast Cancer" *2015 IEEE International Symposium of Antennas and wave Propagation(APS/URSI),* July 2015.

11. **Mahrukh Khan** and Deb Chatterjee, "UWB Microwave Sensor Array Characterization for Early Detection of Breast Cancer" *2015 IEEE Applied Electromagnetic Conference (AEMC),* Dec 2015.

12. Spandana Vemulapalli, **Mahrukh Khan**, and Deb Chatterjee, "Analysis of Ultra-wideband Microwave Imaging via Space Time Beamforming Algorithm in the Frequency Domain," *2015 IEEE Applied Electromagnetic Conference (AEMC),* Dec 2015.

13. **Mahrukh Khan**, "Novel S-Band Phase Modulator Using Hybrid Coupler, *2009 IEEE Asia Pacific Microwave Conference (APMC),* Jan 2009.